ACS OMEGA

http://pubs.acs.org/journal/acsodf

Article

Synthesis and Corrosion Inhibition Performance of Mannich Bases on Mild Steel in Lactic Acid Media

Xiaoyun Zhang,* Yinhang Zhang, Yuxin Su, Xiaoyang Wang, and Renqing Lv

Cite This: *ACS Omega* 2022, 7, 32208−32224

Read Online

ACCESS | Metrics & More | Article Recommendations | Supporting Information

ABSTRACT: Heterocyclic Mannich bases, *N*-(3-oxo-3-phenylpro-pyl)thiazol-2-aminium chloride (DTZA) and *N*-(3-oxo-3-phenylpropyl)-1*H*-pyrazol-3-aminium chloride (DPZA), were developed for the corrosion inhibition of N80 steel in a 15 wt % lactic acid solution. Weight loss measurements, electrochemical techniques, surface characterization, and theoretical calculations were combined to investigate their anticorrosion performance and mechanism. The results showed that DTZA exhibited a satisfactory inhibitor efficiency of 97.56% with a dosage of 0.15% at 363 K, while DPZA achieved only 58.3% under the same conditions. Adsorptions of both inhibitors on the metal surface followed the Langmuir model with physical and chemical adsorptions. Based on X-ray photoelectronic spectroscopy (XPS) analysis, DFT calculations, and molecular dynamics (MD) simulations, stronger interactions between DTZA and iron than those in the case of DPZA were revealed, leading to the formation of a compact protective film on the metal surface, which is attributed to the presence of a thiazole ring in the DTZA chemical structure.

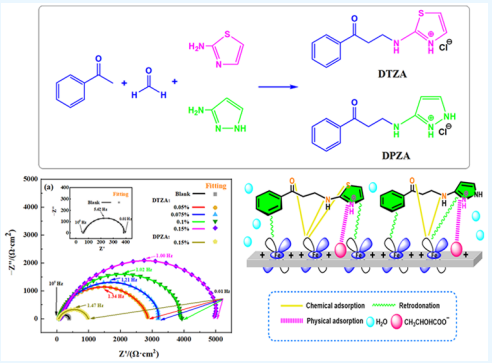

1. INTRODUCTION

In oil and gas industry, hydrochloric acid solely or combined with fluoric acid (mud acid) is widely used as an acidizing fluid due to its low cost and commercial availability.[1] Acids injected into the wellbore can react with carbonate rocks and thus are able to improve the permeability of the subterranean formation.[2,3] However, this conventional acid system has two major drawbacks. First, because the acid−rock reaction is too fast, most of the strong acid is consumed in the near-wellbore zone, thus lowering the acidification efficiency. Second, insoluble salts generated during the acidizing process cause harm to permeability, which is called secondary precipitation.[4] In practice, a mud acid-treated oil well normally undergoes rapid decline after an initial increase in oil production. Therefore, recently, chelating acid systems, which can realize high efficiency and rapid, uniform, and prolonged validity period of acidification, have been developed and have attracted significant attention.[5,6] Recent field applications proved that compared with conventional mud acid acidification, organic chelating acid can simplify the acidification process, reduce the total cost by decreasing the injected acid volume, and achieve a significantly increased production.[7] Organic phosphonic acid, gluconic acid, lactic acid, etc., could be used as chelating acids. Among them, lactic acid can be easily prepared from natural resources such as starch, sugar, etc., by bacterial fermentation methods.[8] It has a wide range of applications in industrial and agricultural fields. When it is used as the main etching agent in acidizing fluids for a formation stimulation operation, lactic acid shows a strong chelating effect on most cationic groups such as Ca^{2+}, Mg^{2+}, Ba^{2+}, etc., thus inhibiting the secondary precipitation of sulfate or carbonate salts.[9] Meanwhile, due to its weak acidity, lactic acid reacts with carbonate rocks slowly during the acidizing process. At the same volume of acids, lactic acid can treat a larger area of a reservoir than mud acid, leading to an improved effect of the acidizing operation. However, there is one big challenge that may prevent lactic acid from having large-scale applications if not properly solved. The acidity of lactic acid (pK_a = 3.8), although not as strong as that of hydrochloric acid, can still cause severe corrosion to metal equipment and tubings. The corrosion rate can be dramatically increased at the well bottom, where the temperature is normally much higher than the ground temperature. Thus, corrosion inhibitors must be added to reduce the aggressive attack of acid on tubing and casing materials during the acidizing process.[10]

There has been a vast amount of research literature on corrosion inhibitors for mild steel in strong acid media.[11] Organic molecules with structural moieties, such as imidazoles,[12] tetrazoles,[13] triazoles,[14] pyridines,[15] quinolones,[16] Shiff bases,[17] Mannich bases,[18] and quaternary ammonium salts[19] have been investigated to serve industrial demands. Among them, Mannich bases prepared from acetophenone, form-

Received: June 7, 2022
Accepted: August 22, 2022
Published: September 1, 2022

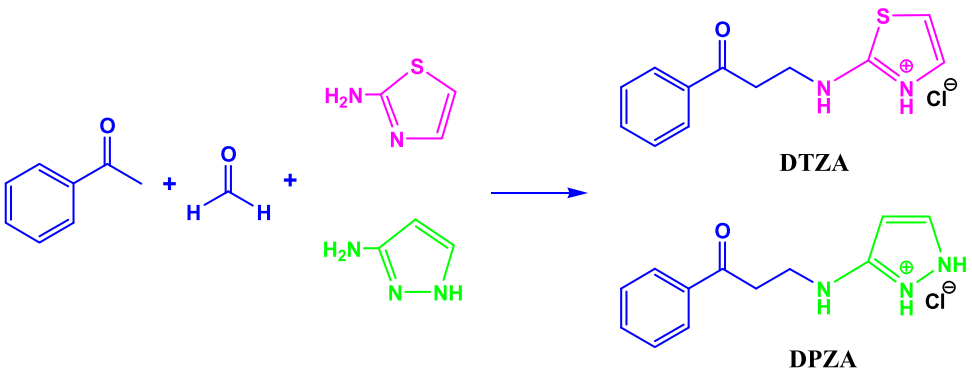

Figure 1. Synthesis of DTZA and DPZA.

aldehyde, and organic amine represent a very important type of corrosion inhibitors used in highly concentrated acid media and at high temperatures.[20,21] Unfortunately, conventional commercial inhibitors that work well in the hydrochloric acid system are unsatisfactory when used in lactic acid. Obviously, lactic acid molecules have a dramatic influence on the formation of a protective layer on a metal surface. Current field applications of chelating acidizing fluids have to use propargyl alcohol or potassium iodide as anticorrosion additives to boost the inhibition performance of the main inhibitor, although both of them are quite expensive and propargyl alcohol is highly toxic.[22]

Although many scientific research studies have been reported on corrosion inhibitors for mild steel, most of them are used in strong acid media, including hydrochloric acid, sulfuric acid, and phosphoric acid.[23,24] Reports on corrosion inhibition of mild steel in lactic acid media are rare. Therefore, aiming at seeking a suitable organic inhibitor for the lactic acid system, in this work, two Mannich base-type corrosion inhibitors, namely *N*-(3-oxo-3-phenylpropyl) thiazol-2-aminium (DTZA) and *N*-(3-oxo-3-phenylpropyl)-1*H*-pyrazol-3-aminium (DPZA), were synthesized. The introduction of the heterocycle into the inhibitor's structure is for increasing the interaction between the inhibitor molecules and the metal surface. The corrosion behavior of the synthesized inhibitors on N80 steel (oil well tubular steel) in lactic acid solution at elevated temperatures was studied, and the inhibition mechanism based on the electronic structure and microscopic adsorption state of the inhibitor molecule was analyzed.

2. EXPERIMENTAL MATERIALS AND METHODS

2.1. Materials. *2.1.1. Synthesis of DTZA and DPZA.* 2-Thiazolylamine (97%, mass percentage concentration, hereinafter unless otherwise indicated) and 3-aminopyrazole (98%) were purchased from Aladdin Chemical Company and used as received. Analytical-grade ethanol (>99.7%), acetone (99%), acetophenone (>99.5%), paraformaldehyde (95%), and GR-grade 37% HCl were acquired from Sinopharm Chemical Reagent Co., Ltd.

As shown in Figure 1, DTZA and DPZA were synthesized through a regular Mannich reaction.[21] Amine (0.0525 mol) was first dissolved in 20 mL of ethanol, to the solution was then added hydrochloric acid (37%) to adjust the pH of the solution to 3−4, and the reaction mixture was stirred for 30 min. After addition of paraformaldehyde (0.075 mol) and acetophenone (0.05 mol), the mixture was stirred continuously at 70 °C for 8 h. The crude product was obtained after the removal of the solvent and then washed with ethanol (10 mL × 3) to obtain the solid. Further purification by column chromatography on silica gel using chloroform/methanol (V/V = 5:1) yielded the final purified product. ^{1}H and ^{13}C NMR spectra of the synthesized Mannich bases were represented in Figures S1−S4 (Supporting Information).

N-(3-oxo-3-phenylpropyl) thiazol-2-aminium chloride (DTZA): white solid. Yield: 73.7%. m.p. 129 °C. ^{1}H NMR (400 MHz, D_2O) δ: 7.55−7.01 (m, 6H), 6.95 (d, 1H), 4.74−4.65 (m, 4H). ^{13}C NMR (400 MHz, D_2O) δ: 170.61, 169.63, 126.99, 126.64, 125.52, 119.58, 118.62, 108.58, 55.67, 42.08. IR (KBr, υ/cm^{-1}) 3074, 2898, 2703, 1608, 763, 709. Elemental analysis: Anal. Calcd for DTZA ($C_{12}H_{13}ClN_2OS$): C, 53.63; H, 4.88; N, 10.42; O, 5.95; S,11.93. Found: C, 53.58; H, 4.92; N, 10.38; O, 5.97; S, 11.97.

O-(3-oxo-3-phenylpropyl)-1*H*-pyrazol-3-aminium chloride (DPZA): yellow solid. Yield: 70.3%. m.p. 212 °C. ^{1}H NMR (400 MHz, DMSO) δ: 8.33 (s, 1H), 7.93 (d, J = 8.9Hz, 2H), 7.77 (s, 1H), 7.63 (d, J = 7.7Hz, 1H), 7.55−7.40 (m, 2H), 3.59−3.52 (m, 2H), 3.45−3.34 (m, 2H). ^{13}C NMR (400 MHz, DMSO) δ: 196.39, 134.28, 133.81, 133.25, 132.48, 128.96, 128.19, 79.81, 38.77, 38.51. IR (KBr, υ/cm^{-1}) 3338, 2930, 2864, 1680, 1583, 1550, 1500, 1446, 754, 701. Elemental analysis: Anal. Calcd for DPZA ($C_{12}H_{14}ClN_3O$): C, 57.26; H, 5.61; N, 16.69; O, 6.36. Found: C, 57.21; H, 5.64; N, 16.72; O, 6.35.

2.1.2. N80 Test Coupons. N80 steel test coupons with a size of 50 mm × 10 mm × 3 mm were used for weight loss and electrochemical studies. The elemental composition of the samples was as follows (in wt %): C(0.35), Cr(0.060), Ni(0.013), Mn(1.53), Mo(0.16), Si(0.37), P(0.016), S(0.045), Al(0.024), V(0.002), Cu(0.08), and Fe (the rest). All steel coupons were consecutively washed in acetone and ethanol, dried at room temperature, and stored in a desiccator prior to use. Test coupons with a 1 cm^2 exposed area were made for electrochemical measurements by covering the rest surface with epoxy resin.

2.1.3. Test Solutions. Lactic acid was used as the etching agent in the corrosion solution.[25] Racemic lactic acid (90%) purchased from Sinopharm Chemical Reagent Co., Ltd. was diluted to 15% with deionized water. When formulated, the Mannich base inhibitor was added directly into the solution with concentrations varied from 0.05 to 0.15%. For the study of weight loss measurements, each test used three steel coupons immersed in 800 g of the acid solution and the weight loss results were averaged.

2.2. Methods. *2.2.1. Weight Loss Measurements.* Weight loss measurements were carried out in a 15% lactic acid solution with different amounts of the inhibitor added at a set

https://doi.org/10.1021/acsomega.2c03545
ACS Omega 2022, 7, 32208−32224

Table 1. Corrosion Parameters Obtained from Weight Loss Tests in 15% Lactic Acid at Different Temperatures

conc.	303 K			333 K			363 K		
wt %	v_{corr} ($g{\cdot}m^{-2}{\cdot}h^{-1}$)	θ	IE (%)	v_{corr} ($g{\cdot}m^{-2}{\cdot}h^{-1}$)	θ	IE (%)	v_{corr} ($g{\cdot}m^{-2}{\cdot}h^{-1}$)	θ	IE (%)
blank	4.67			12.74			32.21		
DTZA									
0.050	0.33	0.929	92.9	1.25	0.902	90.2	6.86	0.787	78.7
0.075	0.13	0.972	97.2	0.39	0.969	96.9	1.42	0.956	95.6
0.100	0.06	0.987	98.7	0.37	0.971	97.1	1.38	0.957	95.7
0.150	0.04	0.991	99.1	0.15	0.988	98.8	0.79	0.976	97.6
DPZA									
0.050	0.83	0.822	82.2	5.63	0.558	55.8	21.02	0.348	34.8
0.075	0.70	0.850	85.0	3.55	0.721	72.1	17.64	0.452	45.2
0.100	0.61	0.869	86.9	2.57	0.798	79.8	15.72	0.512	51.2
0.150	0.20	0.957	95.7	1.42	0.889	88.9	13.43	0.583	58.3

of temperatures from 303 to 363 K. The steel coupons were corroded for 4 h in a 1 L wide-mouth bottle, which contained the formulated acid solution and was kept in a thermostatic water bath, and then were taken out and immediately rinsed with DI water, washed with acetone, dried, and weighed. The average weight loss of the three test coupons was used for the calculation of the corrosion rate (v_{corr}).

$$v_{corr} = \frac{\Delta w}{St} \quad (1)$$

where v_{corr} ($g{\cdot}m^{-2}{\cdot}h^{-1}$) is the corrosion rate, Δw is the average weight loss of the steel samples. S (m^2) is the area of the N80 coupon, and t (h) is the immersion time. Then, the inhibition efficiency (IE) and surface coverage (θ) were determined as follows

$$\text{IE}\ (\%) = \frac{v_0 - v_1}{v_0} \times 100 \quad (2)$$

$$\theta = \frac{\text{IE}\ (\%)}{100} \quad (3)$$

where v_0 and v_1 are the corrosion rates in blank and inhibited solutions, respectively.

2.2.2. Electrochemical Testing Method. A conventional three-electrode system including a working electrode, a platinum counter electrode, and a saturated calomel reference electrode was assembled for electrochemical measurements on an electrochemical workstation (CHI760E). To assure a steady state of the open circuit potential (OCP), the three-electrode system was immersed in the test solution for 1200 s (Figure S5). The AC impedance experiment was performed with the frequency of the current excitation signal in the range from 100 kHz to 10 mHz. Polarization tests were performed in the potential range of −250 to +250 mV with a sweep rate of 1 $mV{\cdot}s^{-1}$. Since the corrosion current density of lactic acid at room temperature and high temperatures varies greatly, a thermostatic water bath was used to control the temperature during measurements. The corrosion potential and the current density were collected by extrapolation at Tafel segments of the polarization curves.[26]

2.2.3. Surface Characterization. Steel coupons treated in the 15% lactic acid solution were used for surface characterization. A scanning electron microscope (SEM, FEI QUANTA FEG250), an atomic force microscope (AFM, SPM-9700), and an X-ray photoelectron spectrometer (XPS, Thermo Fisher, ESCALAB 250Xi) were employed to analyze the surface morphology changes before and after corrosion. Energy-dispersive X-ray spectroscopy (EDX) coupled with the SEM instrument was used to measure the elemental composition of the steel surface.

2.2.4. Contact Angle Measurements. An automatic tensiometer (GERMAN KRUSS DSA30) was used to measure dynamic contact angles at 298 K.

2.2.5. Quantum Chemical Calculations. Quantum chemical calculations were performed using Gaussian 09 software and density functional theory (DFT) by applying the basis set B3LYP/6-311++G(d,p). Multiwfn software was used to further analyze and process the calculation results. Besides, the VMD program was performed to visualize the molecular orbitals and active adsorption sites. Then, the most important quantum chemical parameters such as the dipole moment (μ), the energy of the highest occupied molecular orbital (E_{HOMO}), and the energy of the lowest unoccupied molecular orbital (E_{LUMO}) were determined. In addition, other descriptors including the energy gap (ΔE), hardness (η), and electronegativity (χ) were calculated by the following equations

$$\Delta E = E_{HOMO} - E_{LUMO} \quad (4)$$

$$\chi = \frac{-E_{HOMO} - E_{LUMO}}{2} \quad (5)$$

$$\eta = \frac{E_{LUMO} - E_{HOMO}}{2} \quad (6)$$

The values of ΔN exhibit the path of electron transfer between the corrosion inhibitor molecules and the metal surface, which can be mathematically given as

$$\Delta N = \frac{\chi_{Fe} - \chi_{inh}}{2(\gamma_{Fe} + \gamma_{inh})} \quad (7)$$

where χ_{Fe}, and χ_{inh} are the electronegativities of iron and inhibitor molecules, respectively, and γ_{Fe} and γ_{inh} are the absolute hardness of Fe and inhibitor molecules, respectively. Among them, the theoretically calculated value of χ_{Fe} for the iron metal is taken as 4.82 $eV{\cdot}mol^{-1}$, and γ_{Fe} is 0 $eV{\cdot}mol^{-1}$. These values were appropriately substituted to calculate ΔN.[27]

In addition, the global electrophilic index (ω) is obtained from χ and γ by the following relation[28]

$$\omega = \frac{\chi^2}{2\gamma} \quad (8)$$

2.2.6. Molecular Dynamics Simulations. Materials Studios 2017 was used for molecular dynamics simulation studies. The bulk structure of a 10 × 10 supercell of the Fe (110) surface

https://doi.org/10.1021/acsomega.2c03545
ACS Omega 2022, 7, 32208−32224

was constructed by five layers of 500 pure Fe atoms and was optimized as the iron layer, whereas the solution model contained the inhibitor molecule, 1 $CH_3CHOHCOO^-$, 579 H_2O, 1 H_3O^+, and 19 $CH_3CHOHCOOH$. The water layer was built by 300 H_2O molecules and was frozen to avoid the influence of arbitrary boundary effects. Then, simulations were carried out in a simulation box (24.82 Å × 24.82 Å × 68.04 Å) with a time step of 1 fs and a simulation period of 1000 ps.[29]

3. RESULTS AND DISCUSSION

3.1. Weight Loss Measurements. Weight loss measurement results for N80 steel in the 15% lactic acid solution without and with various concentrations of DTZA and DPZA are listed in Table 1. Since lactic acid is a weak acid, the corrosion rate of a blank solution is much lower than that in hydrochloric acid. As the inhibitor concentration increases, the corrosion rate decreases significantly under the same temperature. Both corrosion inhibitors show corrosion inhibition effects, but DTZA is much better than DPZA at the same level of dosage. At 363 K, when the concentration of DTZA is above 0.075%, the corrosion rates are below 2 $g{\cdot}m^{-2}{\cdot}h^{-1}$. Considering that in practical industry applications, the dosage of corrosion inhibitor is normally in the range of 1−2% (inhibitor concentration of about 10%) and the acceptable corrosion rate in most of the standards is about 4−5 $g{\cdot}m^{-2}{\cdot}h^{-1}$, DTZA could be an efficient corrosion inhibitor in the lactic acid solution. The inhibition efficiency of DPZA at 363 K with a dosage of 0.15% is about 13.43 $g{\cdot}m^{-2}{\cdot}h^{-1}$, apparently not an efficient inhibitor. By the comparison of the DTZA structure with the DPZA structure, it is reasonable to assume that the heterocyclic moiety may play an important role in the enhancement of the inhibition efficiency.

A comparison of the inhibition efficiencies of the two commercial inhibitors with the compounds investigated in the present work can be seen in Table S1 (Supporting Information). To the best of our knowledge, corrosion inhibitors suitable for a lactic acid environment are novel and have not been reported previously. In the presence of 0.15% DTZA, the corrosion rate reached 0.79 $g{\cdot}m^{-2}{\cdot}h^{-1}$ at 363 K in the 15% lactic acid solution, showing better performance than the two propargyl alcohol-added commercial inhibitors.

In the petroleum industry, the well bottom temperature is much higher than the ground temperature. A suitable corrosion inhibitor in acidizing fluids must maintain its inhibition efficiency at elevated temperatures. From Table 1, it is clear that the corrosion rate increases as the temperature increases. The tendency is reasonable because molecules can obtain more energy at higher temperatures; thus, the average kinetic energy increases, which could cause some inhibitor molecules to desorb from the metallic surface.[30] At the same temperature, the steady increase in efficiency with the inhibitor concentration resulted in decreased rates of corrosion. This suggests that increasing concentration plays an important role in enhancing the surface coverage (θ) of DTZA molecules. Besides, the high efficiency of DTZA molecules can be ascribed to the delocalized π-bond of the benzene ring and the thiazole ring that can serve as basic anchor centers to the atoms of the metal. This enables proper coordination with the metal atoms, which leads to an effective surface coverage to isolate the surface from the corrosive medium.[31]

3.2. Electrochemical Impedance Spectroscopy Measurements. The adsorption of inhibitor molecules on the steel surface in 15% lactic acid at 303 K was studied by electrochemical impedance spectroscopy (EIS).[32] To ensure steady-state electrochemical equilibrium, the variation of open circuit potential (OCP) with time was recorded for 1200 s. The variation of the OCP of N80 steel in the 15% lactic acid solution without and with a corrosion inhibitor is given in Figure S5. It is clear that the OCP tended to be stable for 1200 s, and the electrode reached a quasi-steady state in all of the measurements.[33] The Nyquist plots and the Bode plots thus obtained in the absence and presence of DTZA and DPZA in 15% lactic acid are presented in Figure 2. The arc sizes of the capacitive loop are commonly associated with the charge transfer resistance of the N80 steel interface, which can determine whether an inhibitory film is formed on the surface to prevent corrosion. It can be seen that the diameter of the capacitive semicircle increases in the order of increasing inhibitor concentrations (Figure 2a), indicating that the corrosion rate decreases accordingly.[34] The impedance shape remains unchanged due to the identical corrosion mechanism. Compared with DPZA, the diameter of DTZA is significantly larger at the same concentration, revealing that the corrosion inhibition effect of DTZA is better than that of DPZA.

Figure 2b shows impedance moduli with different concentrations of DTZA and 0.15% DPZA. Compared with the uninhibited blank group, both impedance moduli Z increased significantly when the inhibitors were added. The impedance at low frequencies exhibits the typical capacitive reactance, indicating the formation of a well-organized protecting film. As the concentration of DTZA increased, the impedance shifted to the higher frequency region. This behavior can be explained by the better inhibitor coverage of the steel surface. The effect of concentration can also be seen in the Bode phase angle plots (Figure 2c). The phase angle is shifted toward a high value with increased inhibitor concentration. The value of the phase angle reached 65 in the case of 0.15% DTZA, whereas the value is only 35 for DPZA at the same concentration, implying a superior inhibition ability of DTZA to that of DPZA. Besides, the shapes of the Nyquist and Bode plots are similar under different concentrations, which indicates the same mechanism of corrosion. By the comparison of the impedance moduli and phase angles of the two corrosion inhibitors, DTZA is larger than DPZA, indicating that DTZA has a stronger adsorption capacity on the iron surface.

The EIS results were fitted to suitable equivalent electrical circuits (Figure 3), which include the solution resistance R_s, the double-charge layer capacitance CPE_{dl}, the charge transfer resistance R_{ct}, the capacitance of the corrosion product film CPE_f, and the resistance of the corrosion product film R_f. R_p is the sum of R_f and R_{ct}. CPE is the constant phase element of the system of carbon steel in the solution, and the impedance of the CPE is given by[35]

$$Z_{CPE} = Y_0^{-1}(j\omega)^{-n} \tag{9}$$

where Y_0, j, ω, and n stand for the CPE constant, imaginary root, angular frequency, and deviation indicator, respectively. CPE is a physical quantity used to describe the deviation of the parameters of the capacitor, wherefore its parameter Y_0 is the same as the capacitor unit and always takes a positive value.[36] Variable n is connected to the electrode surface homogeneity, and the larger n value of the electrode after adding the inhibitor indicates that the inhibitor molecule is effective and makes the surface smoother. When the value of n is close to 1, the CPE can be regarded as an ideal capacitor with a polished

https://doi.org/10.1021/acsomega.2c03545
ACS Omega 2022, 7, 32208−32224

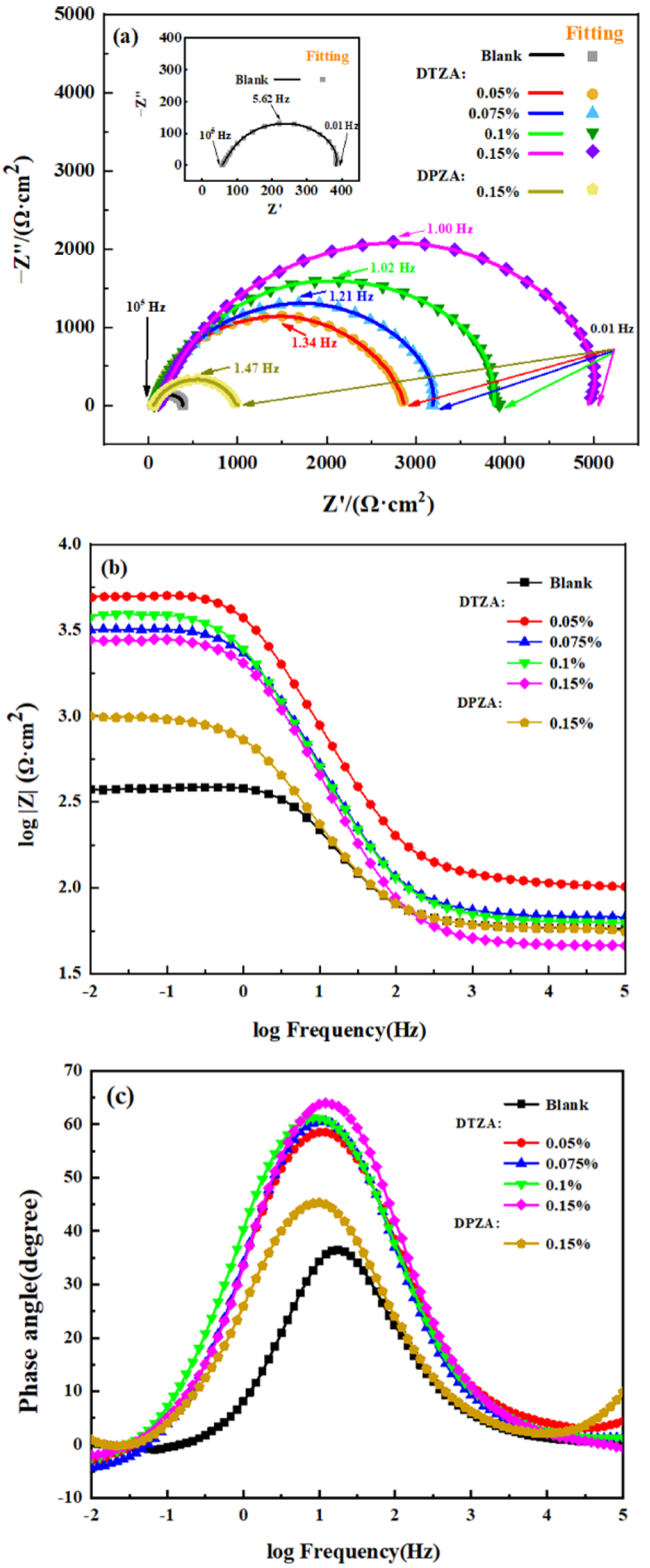

Figure 2. Electrochemical impedance plots for inhibitors DTZA and DPZA at 303 K: (a) Nyquist plots, (b) Bode modulus plots, and (c) Bode phase angle plots.

surface, and CPE is able to behave as a resistor when the value of n is 0. The numerical results of n between 0 and 1 in Table 2 reflect intermediate behavior between a capacitor and a resistor.[37] In Figure 2b, the line is drawn by the test data, while the scattered points are the fitting data. It can be observed that the experimental and fitted impedance data superimposed perfectly on each other, indicating the validity of the equivalent electrical circuits adopted for the simulation of the electrochemical impedance data. The fitted data are shown in Table 2. The high fitting quality of the data is achieved by sufficiently small chi-square values (χ^2) in orders of 10^{-3} and 10^{-4}, indicating that the fitting error is quite small and the equivalent models used have high accuracy. The double-layer capacitance (C_{dl}) for nonideally polarized electrodes with irreversible charge transfer is estimated via the following formula[38]

$$C_{dl}(\mathrm{F\cdot cm^{-2}}) = Y_{0,dl}^{1/n}\left(\frac{1}{R_s} + \frac{1}{R_{ct}}\right)^{n-1/n} \tag{10}$$

$$C_f(\mathrm{F\cdot cm^{-2}}) = Y_{0,f}^{1/n} \times R_f^{1-n/n} \tag{11}$$

The values of $Y_{0,dl}$ and C_{dl} listed in Table 2 decrease in the presence of DTZA and DPZA, probably owing to the adsorption of both inhibitors facilitating the displacement of primarily adsorbed molecules, especially water molecules, thereby reducing the local dielectric constant and increasing the boundary thickness at the electric double layer. Helmholtz defined a formula to express the double-layer capacitance, in terms of electrode surface (S), the permittivity of air (ε_0), local dielectric constant (ε), and film thickness (d), which is given as follows[39]

$$C_{dl} = \frac{\varepsilon\cdot\varepsilon_0}{d}S \tag{12}$$

Therefore, corrosion inhibitor molecules compete to adsorb and replace water molecules on the metal surface so that the dielectric constant (ε) is reduced, and a dense protective film is formed, thereby increasing the film thickness (d), leading to a lower value for C_{dl}. The corrosion inhibition performance (IE) based on the charge transfer resistance was calculated by the following equation[40]

$$\mathrm{IE}\ (\%) = \frac{R_{ct} - R_{ct}^0}{R_{ct}} \times 100 \tag{13}$$

where R_{ct} and R_{ct}^0 are the charge transfer resistances with and without inhibitors, respectively. It can be clearly seen from Table 2 that the charge transfer resistance (R_{ct}) and the values of R_p improve with the corrosion inhibitor concentration, which is inversely proportional to the corrosion rate, demonstrating that a protective film was formed on the metal surface by adsorption, which created a stronger barrier at active sites. Therefore, the transfer of charges from the metal surface to the corrosive medium becomes more difficult. Apart from this, with the two corrosion inhibitors at the same concentration, the charge transfer resistance of DTZA is greater, implying that the inhibition performance of DTZA is better than that of DPZA. At a dosage of 0.15%, DTZA provided a maximum IE % of 93.43% in the whole investigated range.

The relaxation time is the time required to characterize a certain variable of the system from a transient state to a certain steady state. The characteristic constant (f_0) is used to obtain the relaxation time constant τ_0 by the following relation[41]

$$\tau_0 = \frac{1}{2\pi f_0} \tag{14}$$

https://doi.org/10.1021/acsomega.2c03545
ACS Omega 2022, 7, 32208−32224

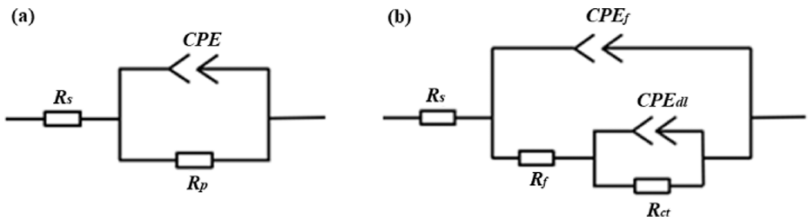

Figure 3. Equivalent circuit of electrochemical impedance spectroscopy: (a) without inhibitors and (b) with inhibitors.

Table 2. Electrochemical Parameters Obtained from EIS Data for the N80 Sample in a 15% Lactic Acid Solution Containing Different Concentrations of DTZA and 0.15% DPZA at 303 K

		DTZA				DPZA
parameters	blank	0.05%	0.075%	0.10%	0.15%	0.15%
R_s ($\Omega\cdot cm^{-2}$)	59.05	46.35	68.16	63.16	101.9	58.20
R_{ct} ($\Omega\cdot cm^{-2}$)	339.5	2765	3170	3950	5169	841.3
$Y_{0,dl} \times 10^5$ ($\Omega^{-1}\cdot s^n\cdot cm^{-2}$)	14.6	2.45	2.45	2.88	2.55	7.32
n_{dl}	0.81	0.87	0.85	0.83	0.83	0.81
$C_{dl} \times 10^6$ ($F\cdot cm^{-2}$)	46.1	8.87	7.90	7.88	7.50	2.00
R_f ($\Omega\cdot cm^{-2}$)		36.81	50.99	52.05	35.03	58.30
$Y_{0,f} \times 10^5$($\Omega^{-1}\cdot s^n\cdot cm^{-2}$)		3.47	3.02	3.21	1.01	4.14
n_f		0.88	0.87	0.86	0.84	0.84
$C_f \times 10^7$($F\cdot cm^{-2}$)		52.3	35.4	31.3	5.74	13.1
R_p ($\Omega\cdot cm^{-2}$)		2801	3220	4002	5204	899.6
τ_0 (ms)	28.32	118.77	131.53	156.03	159.15	59.65
$\chi^2 \times 10^4$	38.0	4.12	10.3	6.98	17.4	1.13
IE (%)		87.7	89.3	91.4	93.4	59.7

As the DTZA concentration increases from 0.05% to 0.075%, 0.1%, and 0.15%, the corresponding τ_0 values show an increasing tendency from 118.77 ms to 131.53 ms, 156.03 ms, and 159.15 ms, respectively. All values are significantly larger than the τ_0 value (28.32 ms) of the uninhibited lactic acid solution. This indicates that the charge transfer process of the metal is largely slowed down after the addition of DTZA, and the surface of the mild steel is well protected. The τ_0 value with 0.15% DPZA is calculated to be 108.27 ms, which is smaller than that of DTZA at the same concentration, indicating that DPZA has an inferior ability to hinder the loss of electrons on the iron surface.

3.3. Potentiodynamic Polarization Curves. The polarization curves were obtained from the N80 coupons immersed in 15% lactic acid solutions. Since the corrosion current density of lactic acid is low at room temperature, the tests were carried out at 363 K. It is visible from Figure 4 that the corrosion current densities of the cathode and the anode decrease after adding the inhibitors to the acid solution. The decrease is more obvious in the case of DTZA than that in DPZA at the same concentration, meaning that the former has greater inhibition capacity. Both inhibitors behave as mixed-type inhibitors because both the anodic and cathodic curves move toward the lower current density. The shapes of all cathodic and anodic curves do not change compared with blank, indicating that the reaction mechanisms of cathode oxygen reduction and the anode dissolution reaction stay unchanged. The related kinetic parameters including corrosion current density (I_{corr}), corrosion potential (E_{corr}), anodic Tafel slopes (β_a), cathodic Tafel slopes (β_c), polarization resistance (R_p), and inhibition efficiency (IE%) were calculated and are listed in Table 3. The inhibition efficiency was estimated by the following equation[42]

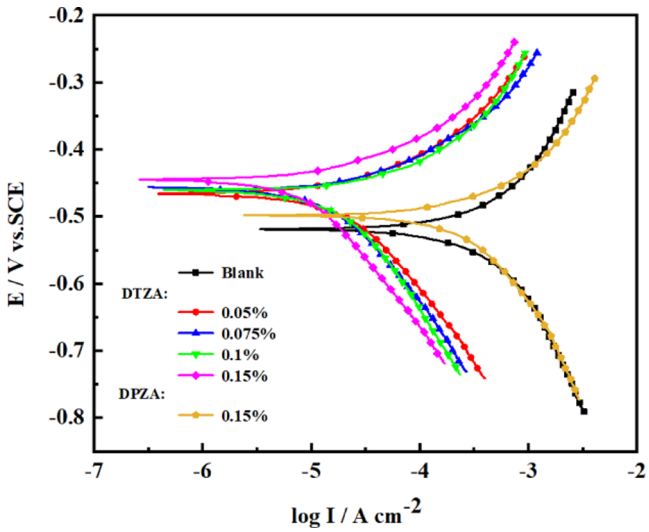

Figure 4. Polarization curves for N80 steel measured with different concentrations of DTZA and 0.15% DPZA at 363 K.

$$IE\% = \frac{I_{corr}^0 - I_{corr}}{I_{corr}^0} \times 100 \quad (15)$$

where I_{corr}^0 and I_{corr} denote the corrosion current densities for N80 steel without and with inhibitors, respectively. As shown in Table 3, the anodic and cathodic Tafel slopes (β_a and β_c) change with inhibitor concentration, implying that the inhibitor affects both the cathodic and anodic reactions. For both DTZA and DPZA, the deviation in corrosion potential E_{corr} lies below 85 mV, and the corrosion inhibitors can be classified as mixed-type.[43,44] As the concentration of DTZA increases from 0.05 to 0.15%, the I_{corr} value of N80 steel in

https://doi.org/10.1021/acsomega.2c03545
ACS Omega 2022, 7, 32208−32224

Table 3. Electrochemical Parameters Obtained from Polarization Curves for N80 Steel in a 15% Lactic Acid Solution Containing Different Concentrations of DTZA and 0.15% DPZA at 363 K

inhibitor	C (wt %)	β_c (mV·dec^{-1})	β_a(mV·dec^{-1})	I_{corr} (μA·cm^{-2})	E_{corr} (V)	R_p (Ω·cm^{-2})	IE%
blank	0	−4.805	5.336	455.8	−0.519	43.17	
DTZA	0.05%	−4.904	6.405	116.5	−0.460	74.67	74.4
	0.075%	−5.426	7.698	74.17	−0.465	106.38	83.7
	0.1%	−5.415	7.692	68.99	−0.466	113.80	84.9
	0.15%	−5.295	8.022	42.55	−0.444	157.11	90.7
DPZA	0.15%	−5.278	6.187	409.2	−0.497	49.58	10.2

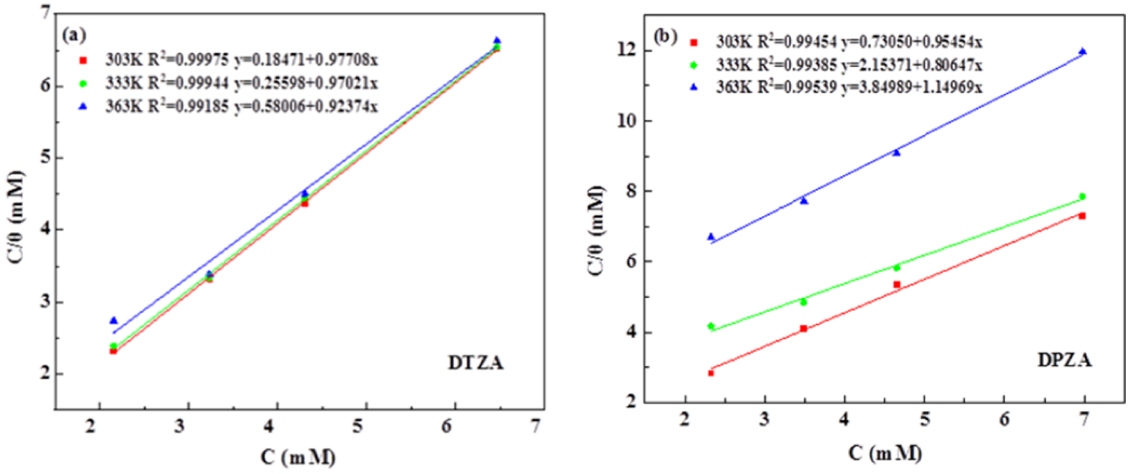

Figure 5. Langmuir adsorption curves of DTZA (a) and DPZA (b) for N80 steel in a 15% lactic acid solution at different temperatures.

lactic acid decreases from 116.5 to 42.55 μA/cm^2, the corresponding polarization resistance R_p increases from 74.67 to 157.11 Ω, and the inhibition efficiency IE increases from 74 to 90.7%. This finding suggests that both the anodic and cathodic reactions have been suppressed. DTZA has an excellent ability to inhibit mild steel corrosion in the lactic acid solution. In contrast, 0.15% DPZA can only achieve an inhibition efficiency of 10.2%.

3.4. Adsorption Isotherm and Thermodynamic Parameters. The adsorption of inhibitors on steel in the lactic acid solution can be a substitution process of the absorbed water molecules on the metal surface by added inhibitor molecules. Test data obtained from weight loss measurements were used to fit several adsorption isotherm models, and the Langmuir adsorption isotherm was found to be the best fit, which is shown as follows

$$\frac{C_{inh}}{\theta} = \frac{1}{K_{ads}} + C_{inh} \quad (16)$$

where C_{inh}, θ, and K_{ads} are the inhibitor concentration, the surface coverage of the inhibitor, and the equilibrium constant of the adsorption/desorption process, respectively. The linear relationship between C and C/θ is represented in Figure 5. The linear regression coefficient (R^2) nearly equals 1 for all inhibitors, indicating that the corrosion inhibitor molecules are adsorbed in a monolayer on the iron surface.

Moreover, the equilibrium constant K_{ads} values were 1724 and 260 for DTZA and DPZA at 363 K, respectively. The relatively high value of K_{ads} implied that DTZA could adsorb firmly on the metal surface. The adsorption-related parameters of DTZA at different temperatures are shown in Table 4. It can be seen obviously that the values of K_{ads} gradually decrease with the increase of the temperature ranging from 303 to 363 K. As the temperature increases, the kinetic energy of the molecules increases, leading to a decrease in the adsorption capacity of the metal surface. From constant K_{ads}, the adsorption free energy ΔG_{ads} can be determined as follows[45]

$$\Delta G_{ads} = -RT \ln(55.5K_{ads}) \quad (17)$$

where R is the universal gas constant, T is the thermodynamic temperature, and 55.5 is the molar concentration of water.[45] The calculated ΔG_{ads} values of DTZA and DPZA in a 363 K environment are −34.62 and −28.90 kJ·mol^{-1}, respectively. The adsorption energy of DTZA is more negative than that of DPZA. This could serve as evidence of its stronger adsorption.

Table 4. Adsorption Parameters of DTZA and DPZA on the Mild Steel Surface in 15% Lactic Acid at Different Temperatures

inhibitor	temp. (K)	K_{ads} (M^{-1})	ΔG_{ads} (kJ·mol^{-1})	slope	R^2
DTZA	303	5414	−31.78	0.97708	0.99971
	333	3907	−34.02	0.97021	0.99948
	363	1724	−34.61	0.92374	0.99178
DPZA	303	1369	−28.31	0.95454	0.99454
	333	464	−28.12	0.80647	0.99385
	363	260	−28.90	1.14969	0.99539

3.5. SEM and EDX Analysis. Figure 6 shows the SEM images and relevant EDX analysis of the metal surface treated in uninhibited and inhibited test solutions (15% lactic acid) for 4 h at 363 K. Figure 6a represents the image of a mechanically polished smooth surface before the acid treatment. Figure 6b shows the image of the steel coupon immersed in the acid solution without a corrosion inhibitor, which is rough and badly damaged due to severe corrosion in the acid medium. The corresponding EDX analysis shows 10.48% O content,

https://doi.org/10.1021/acsomega.2c03545
ACS Omega 2022, 7, 32208−32224

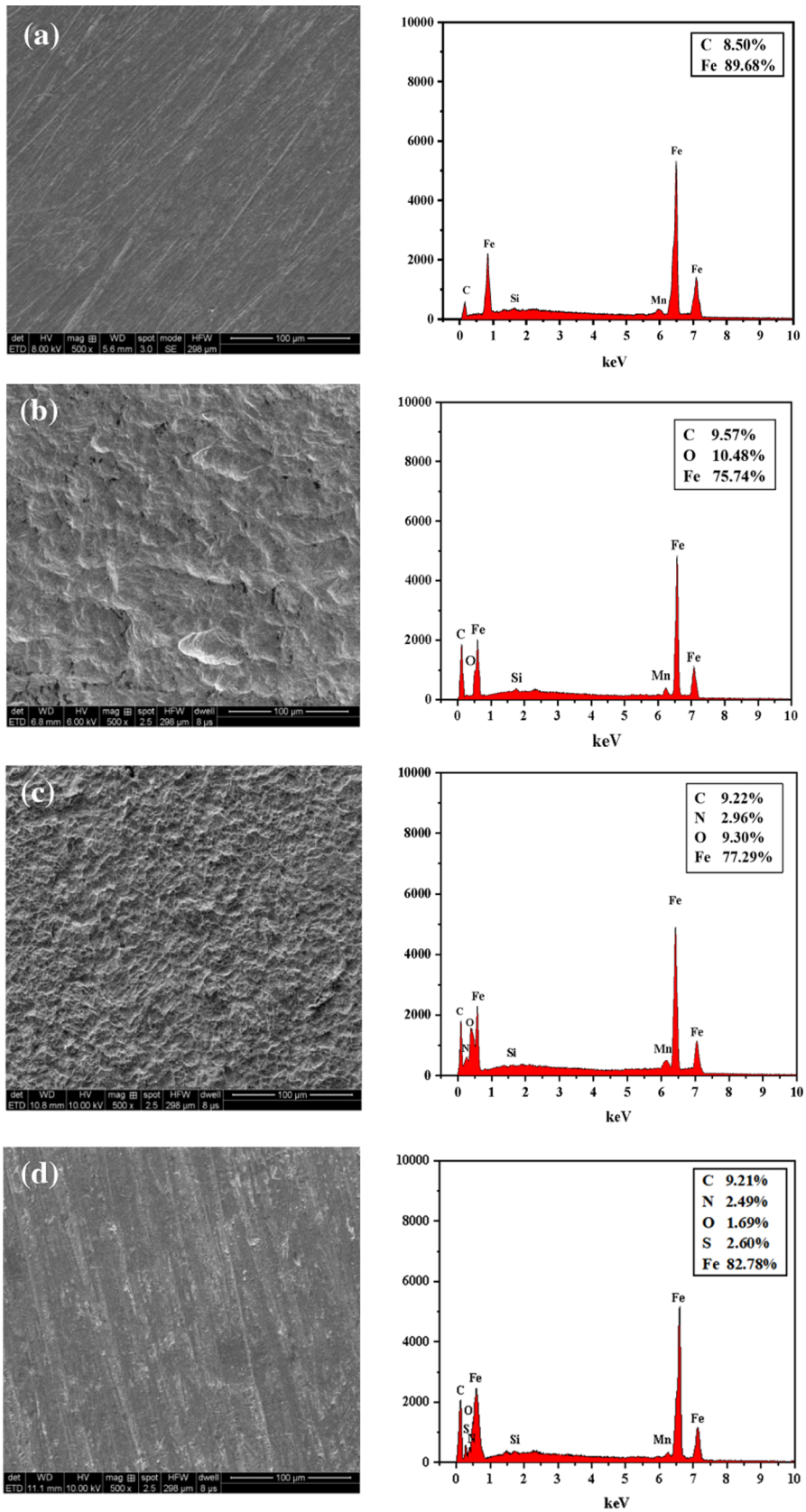

Figure 6. SEM images and their corresponding EDX analysis of N80 steel before (a) and after 4 h immersion in a 15% lactic acid solution uninhibited (b) and inhibited with 0.15% DPZA (c) and DTZA (d) at 363 K.

indicating that the metal surface may be covered by many corrosion products. Figure 6c shows a much better surface imaged with 0.15% DPTA, although still many smaller pits are observed. A protective film may be formed on the iron surface

https://doi.org/10.1021/acsomega.2c03545
ACS Omega 2022, 7, 32208−32224

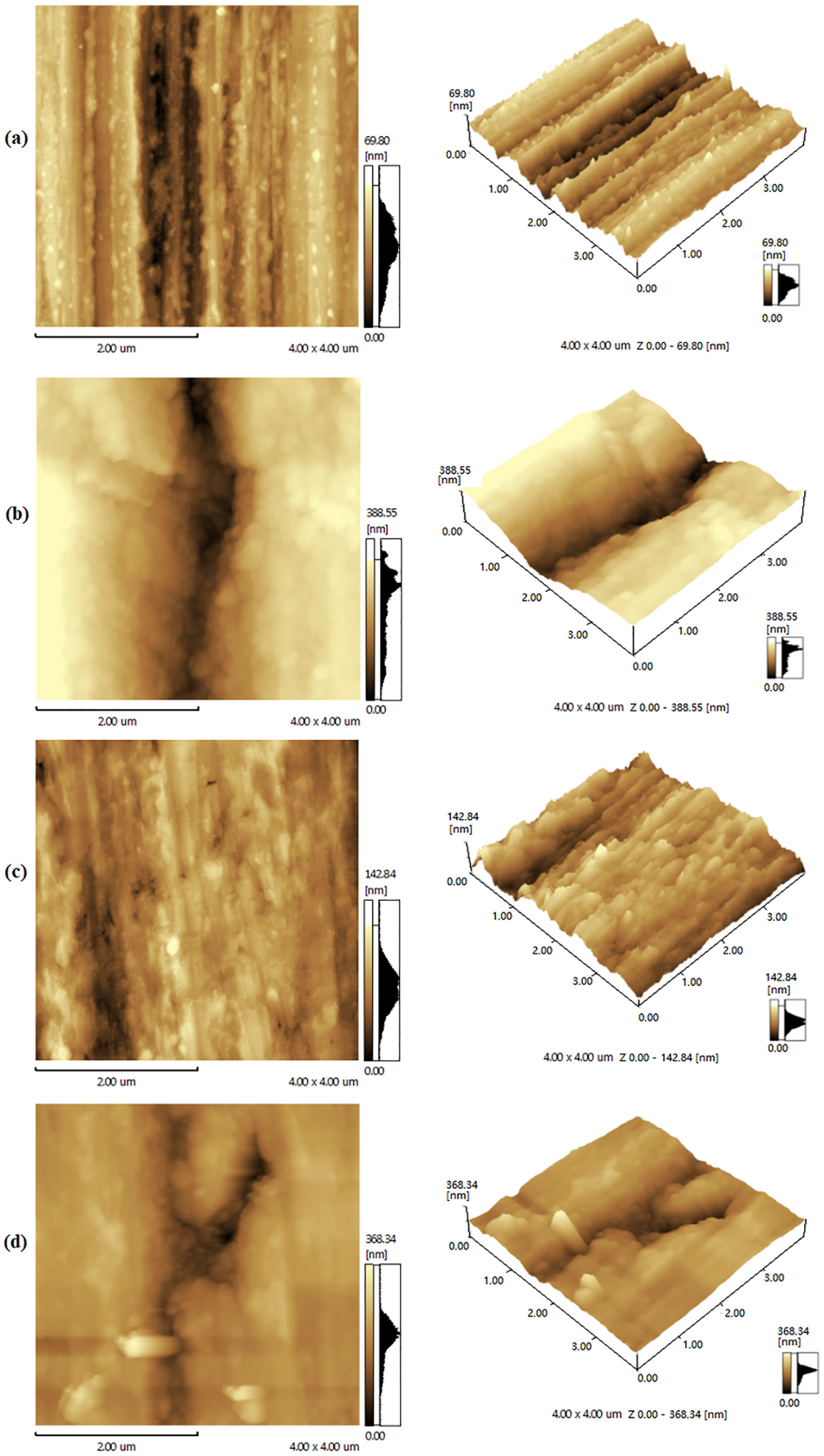

Figure 7. 2D and 3D images of AFM for N80 steel specimens on the freshly ground steel surface (a), after immersion in 15% lactic acid solution (b), and inhibited with 0.15% DTZA (c) and DPZA (d) in a 15% lactic acid solution after 4 h immersion at 363 K.

to isolate the metal from the corrosive medium, which is evidenced by the appearance of 2.96% N. In contrast, the steel surface treated in the presence of 0.15% DTZA is very smooth. In Figure 6d, some scratches that are attributed to the

https://doi.org/10.1021/acsomega.2c03545
ACS Omega 2022, 7, 32208−32224

Table 5. Roughness Parameters of DTZA and DPZA on the Mild Steel Surface in 15% Lactic Acid after 4 h Immersion at 363 K

medium	average roughness (R_a)	RMS roughness (R_q)	maximum profile valley depth (R_v)
	10.796 nm	13.299 nm	38.229 nm
15% lactic acid	83.435 nm	98.797 nm	265.708 nm
15% lactic acid + 0.15% DTZA	17.281 nm	21.362 nm	75.672 nm
15% lactic acid + 0.15% DPZA	34.522 nm	45.252 nm	196.926 nm

mechanical polishing are also visible, meaning that the surface is well protected by the corrosion inhibitor. The corresponding EDX spectrum shows the characteristic peaks of N and S, implying that the DTZA molecules are effectively adsorbed on the N80 steel surface to prevent aggressive attachment. These results are consistent with those obtained from weight loss and electrochemical measurements.

3.6. AFM Analysis. Figure 7 shows the 2D and 3D AFM images of the N80 steel surfaces including polished bare iron samples and three test samples corroded in the 15% lactic acid solution with and without an inhibitor (DTZA or DPZA). The average roughness (R_a), the root mean square (R_q), and the maximum profile valley depth (R_v) are listed in Table 5. The bare polished coupon surface expressed the values of R_a, R_q, and R_v as 10.796, 13.299, and 38.229 nm, respectively. Note that the slight roughness on the surface of the fresh steel sheet may be attributed to scratches left during polishing and curing corrosion when exposed to air. In contrast, the values of R_a, R_q, and R_v for the uninhibited carbon steel surface are 83.435, 98.797, and 265.708 nm, respectively. This result suggests that the surface of blank steel is very rough due to the attack of the high-temperature acid solution. Especially, the steel coupon immersed in the test solution containing DTZA showed a smoother and much denser surface morphology, meaning that the DTZA molecules are easier to form a denser adsorption layer to block the corrosive medium from reaching the steel surface.[46] The DTZA inhibitor has excellent inhibition performance compared to DPZA, and the argument is supported by the previous results of the weight loss measurement, EIS, and SEM observation.

3.7. XPS Analysis. The chemical properties of the surface of the N80 steel sheet after the static weight loss experiment were analyzed by XPS technology, including elemental composition, element chemical state, and electronic state, and then the adsorption of high-performance organic DTZA molecules on the iron surface was evaluated. The full XPS spectrum of the surface layer of the metal is shown in Figure 8a, which contains peaks of Fe, O, C, N, and S, which are related to the main components of the investigated steel sheet, the main components of corrosion products, and the constituent elements of the corrosion inhibitor molecules. Figure 8b shows an Fe 2p spectrum after peak fitting. The first peak of the test results can be compared to two peaks of 710.5 and 713.4, indicating that the Fe element is FeOOH and iron oxides (Fe_2O_3, Fe_3O_4) at the above binding energies, respectively.[47] Besides, satellite peaks of Fe (III) and the existence of free Fe^{3+} are assumed to have a single peak at 719.6 and 724.6, respectively.[48] The O 1s spectrum (Figure 8c) has two peaks near 530, between which the peak at 529.8 mainly contributes to the formation of iron oxides FeO, Fe_2O_3, and Fe_3O_4, while the only peak at 531.4 contributes to the presence of −C−O and −OH, which corresponds to the spectrum of Fe 2p.[49] The physical barrier of corrosion products separates the iron surface from the corrosive environment, preventing further corrosion. The test curve of the N 1s spectrum can be fitted with three single peaks, as shown in Figure 8d. Among them, the single peak at 398.1 relates to the structures of −C—N and −C═N−, which is consistent with the protonated N on the thiazole ring and C−N bonds in the molecular structure of DTZA, and the second single peak is located at 399.6, indicating that the lone electron pair of each N atom contributes with the empty orbital of iron to form a coordination group. The third peak at around 400 demonstrates that the DTZA inhibitor molecule acts as a protonated N in the Mannich base hydrochloride structure.[50] Figure 8e shows the C 1s spectrum, composed of three single peaks. The peak at 284.8 indicates the possible presence of C−C, C−H, and C═C, and the peak at 285.2 can prove the occurrence of C−N and C═N, reflecting the presence of the thiazole ring of the DTZA molecule, and the peak at 288.5 indicates the presence of C═O, which matches the carbonyl component of DTZA.[51] The thin-scan S 2p spectrum of S, the unique constituent element of DTZA as a corrosion inhibitor molecule, is shown in Figure 8f. The peak at a binding energy of 162.8 corresponds to the formation of C−S, and the peak at a binding energy of 168.4 corresponds to the presence of Fe−S groups,[52] which indicates that DTZA molecules are adsorbed on the N80 steel sheet via the corrosion process, and the S atoms form a bond complex with the iron surface. This not only blocks the corrosion medium but also protonates the corrosion inhibitor molecules, interacts with the free electrons on the metal surface electrostatically, and reduces the charge exchange between the metal and the solution. Thus, the corrosion inhibition performance of DTZA is excellent, which is consistent with the experimental results.

3.8. Contact Angle Measurements. The contact angle was measured to analyze the hydrophobic/hydrophilic property of the N80 steel surface before and after treatment in acid solution. Generally, a value of the contact angle less than 90° means that the metal surface is hydrophilic, whereas a value of more than 90° means that the metal surface is hydrophobic.[53] As shown in Figure 9a, the contact angle of the freshly polished steel sheet was 105°, and the value changed to 42° after being immersed in the lactic acid solution without inhibitors for 4 h at 363 K, suggesting that the increase in surface wettability was due to the acid attack on the steel surface. In the presence of 0.15% DTZA or DPZA, the contact angles increased to 137 and 79°, respectively. The high value of contact angle for DTZA compared to DPZA could be attributed to the products formed by DTZA molecules on the iron surface, which may displace water molecules on the metal/solution interface more effectively, thus forming a more effective protection film.

3.9. Quantum Chemical Calculation. Quantum chemical calculation was performed to reveal the correlation between the molecular structure and the anticorrosion performance for DTZA and DPZA. Prior to the calculation, Marvin Sketch software was employed to verify the true states of DTZA and

https://doi.org/10.1021/acsomega.2c03545
ACS Omega 2022, 7, 32208−32224

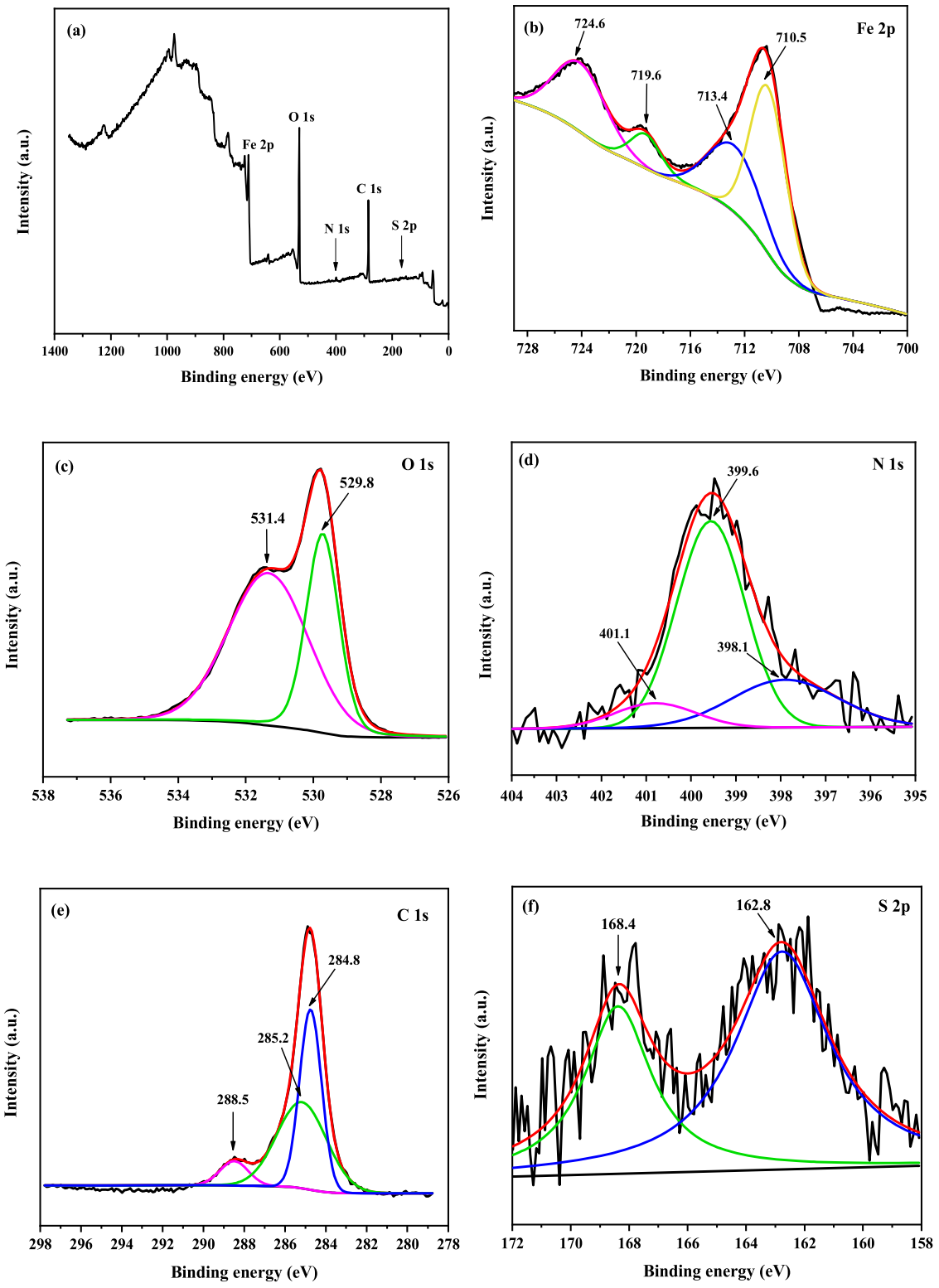

Figure 8. XPS spectrum of the surface scraped from the N80 steel sheet after adding DTZA in 15% lactic acid at 363 K: (a) full spectrum and narrow spectrum tests of (b) Fe, (c) O, (d) N, (e) C, and (f) S elements.

DPZA in the pH range of 0−14 (Figure 10).[54] The pH values of the 15% lactic acid solution are 1.57 and 1.13 at 298 and 363 K, respectively. Referring to Figure 10, DTZA and DPZA molecules should exist in protonated forms in the lactic acid; thus, their neutral forms and protonated forms at N other than cyclic imino N could be neglected. This is reasonable because the protonated thiazole and pyrazole rings have more stable resonance structures than that protonated at acyclic N. Therefore, the following DFT analysis was performed on DTZA and DPZA in their protonated states rather than neutral forms.

Figure 11 displays the optimized structures and HOMO and LUMO distributions of DTZA and DPZA. Their HOMOs fall on the benzene ring. However, the LUMO of DPZA is located

https://doi.org/10.1021/acsomega.2c03545
ACS Omega 2022, 7, 32208−32224

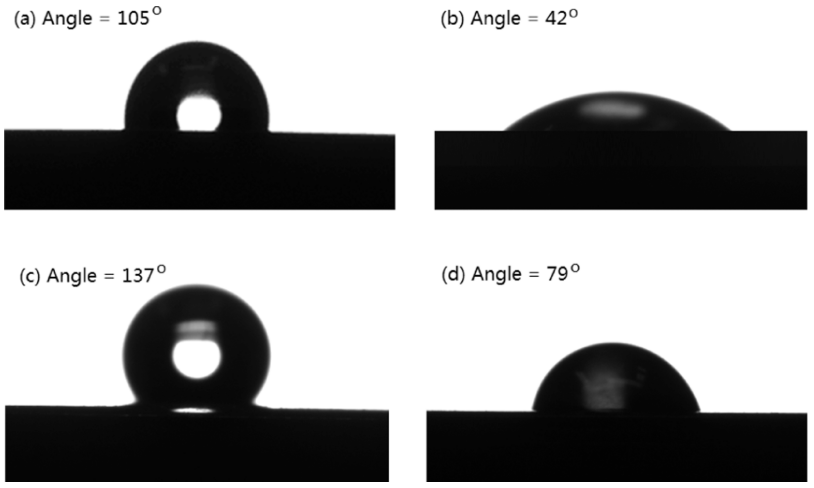

Figure 9. Cross-sectional optical images of water droplets on a fresh steel surface (a), after immersion in a blank acid solution (b), and in a 15% lactic acid solution inhibited with 0.15% DTZA (c) and DPZA (d) at 363 K.

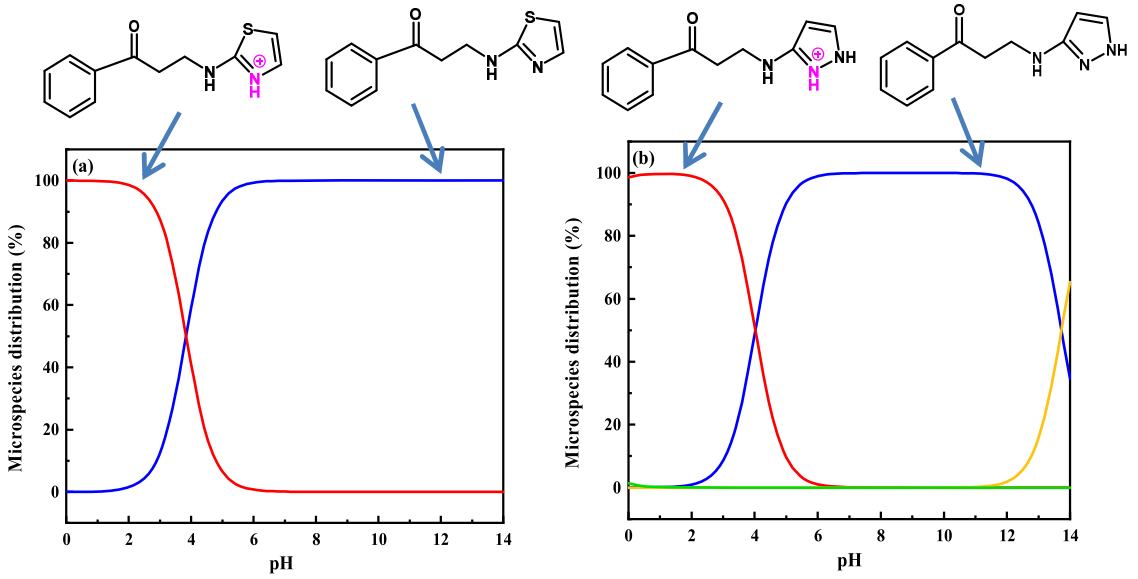

Figure 10. Microspecies distribution of DTZA (a) and DPZA (b) at different pH values.

on the positively charged five-membered ring, whereas the LUMO of DTZA also includes the benzene ring. Herein, the large π bond of the benzene ring can be regarded as a buffer system with both electron-withdrawing and electron-donating capabilities.[55] The parameters[56] such as E_{HOMO}, E_{LUMO}, dipole moment (μ), energy gap (ΔE), electronegativity (χ), global hardness (γ), and the fraction of electrons transferred from inhibitor molecules to the metal atoms (ΔN) are listed in Table 6. It is generally believed that the energy value of the HOMO (E_{HOMO}) is related to the tendency of the inhibitor to donate electrons to unoccupied Fe orbitals, and conversely, E_{LUMO} is associated with the ability of the inhibitor to accept electrons from the Fe surface.[57] Then, a large E_{LUMO} value and the E_{LUMO} value indicate the strong adsorption capacity of the molecule to the metal surface. As shown in Table 6, the E_{HOMO} of DTZA is larger than that of DPZA, indicating that the DTZA molecule has a stronger electron-donating ability,[58] which may be related to the contribution of the sulfur atom. The slightly negative E_{LUMO} of protonated DPZA may be attributed to its more adsorption sites. In addition, the lower ΔE of DTZA in the protonated states indicates the higher reactivity of the inhibitor, demonstrating that DTZA molecules have strong adsorption capacity and can form a dense adsorption layer on the surface of the N80 steel sheet.[59] The ΔN values of both inhibitors are negative, indicating that electrons are transferred from the iron atoms to inhibitor molecules. In this way, the inhibitor molecules are absorbed on the metal surface. DTZA has a more negative ΔN value, possibly meaning that it has more electrons transferred than DPZA. As for the dipole moment, DTZA has a larger value of μ than DPZA. But the question of whether a larger μ should favor or disfavor an increased inhibition efficiency is not clear. Some researchers have shown that the increase in μ leads to an increased inhibition efficiency,[60] while others say the contrary.[61] Additionally, according to the principle of "Hard and Soft Acid–Base (HSAB)" proposed by Hackerma,[62] the N80 carbon steel matrix is considered to be a soft acid, so it can form covalent bonds with soft and basic corrosion inhibitors for adsorption.[63] DTZA has a smaller hardness (γ) value than DPZA, illustrating that its excellent deformation ability leads to less steric hindrance, which is helpful to its adsorption on the N80 steel surface. This may also stand for its

https://doi.org/10.1021/acsomega.2c03545
ACS Omega 2022, 7, 32208−32224

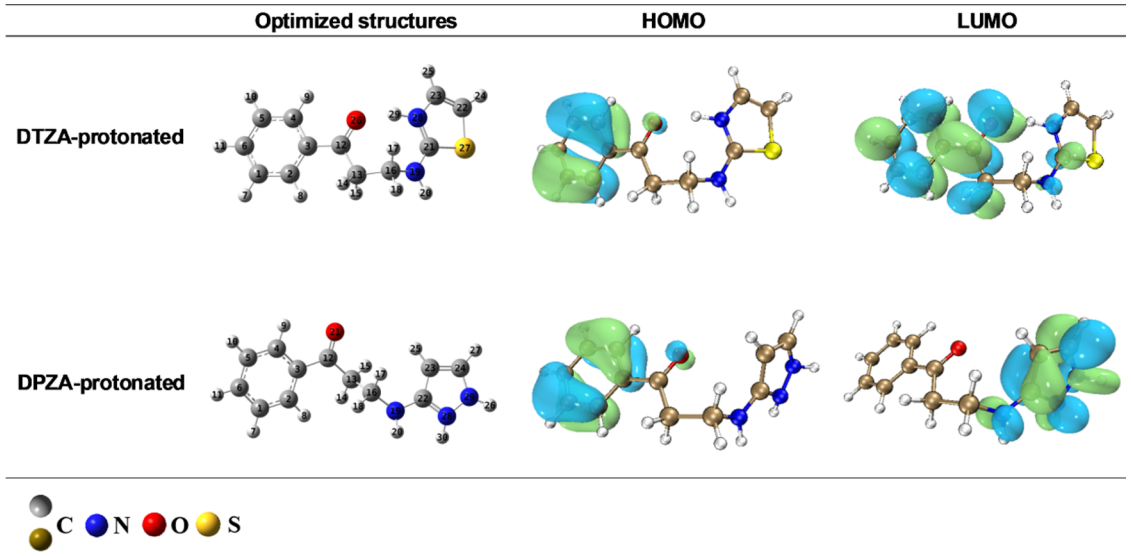

Figure 11. Optimized geometry structures and the frontier molecule orbital density distributions of protonated DTZA and DPZA.

Table 6. Quantum Chemical Parameters of DTZA and DPZA

parameters	DTZA (protonated)	DPZA (protonated)
E_{HOMO} (eV)	−9.6791	−9.9910
E_{LUMO} (eV)	−5.4288	−5.2005
ΔE (eV)	4.2503	4.7905
μ (Debye)	9.9721	8.2882
χ (eV)	7.5540	7.5958
γ (eV)	2.1252	2.3953
ΔN	−0.6432	−0.5794
ω (eV)	13.4253	12.0436

better inhibition efficiency. The global electrophilic index (ω) is used to judge the nucleophilic or electrophilic reactivity of the inhibitors. The ω value of protonated DTZA is 13.4253 eV, greater than that for DPZA (12.0436 eV) in the same state, indicating that DTZA has a greater reduction in the system energy in obtaining electrons. Therefore, DTZA behaves as a stronger electrophile.

To further study the electrostatic interaction between the inhibitor and the N80 steel surface, the electrostatic potential (ESP) analysis was performed.[64] Figure 12 illustrates the ESP distribution of DTZA and DPZA molecules in protonated states. The red and blue areas indicate the negatively and positively charged regions, corresponding to the possible electrophilic and nucleophilic reaction centers, respectively. The entire electrostatic potential distribution of protonated molecules is positive. Among them, the positivity distribution

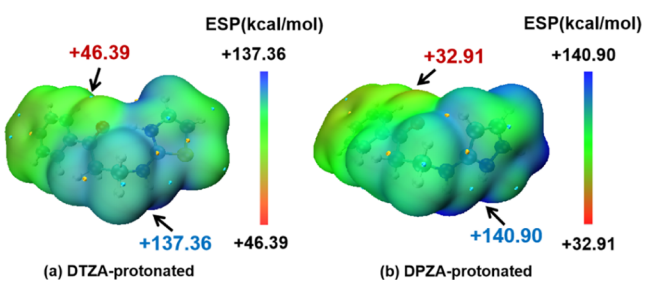

Figure 12. Electrostatic potentials of DTZA (a) and DPZA (b).

of DTZA ranges from +46.39 to +126.75 kcal/mol, which is on average higher than that of DPZA (+32.91 to +140.9 kcal/mol), indicating that protonated DTZA behaves as a reagent with good electrophilicity.[65] This indicates that the protonated molecules can electrostatically attract the surface of the soft acidic metal substrate and perform physical adsorption to replace the lactate anions adsorbed on the metal surface, forming an excellent mechanical barrier. Protonated DTZA molecules are more electropositive and therefore are more effective at protecting the metals from corrosion.

3.10. Molecular Dynamics (MD) Simulations. Molecular dynamics simulations were used to visually simulate the adsorption process of the corrosion inhibitor molecules on the metal surface. The structures of water, 15% lactic acid solution layer, corrosion inhibitor molecule, and Fe (110) surface models were constructed and optimized before simulations. The entire system reached an equilibrium state by balancing energy and temperature. The top and side views of DTZA and DPZA in protonated states after adsorption equilibrium are shown in Figure 13. It is clear that the inhibitor molecule is almost adsorbed on the iron surface in parallel orientation. This parallel mode can maximize the contact area of the inhibitor and the Fe substrate, hence increasing the surface coverage for a single molecule. Additionally, the adsorption strength of the inhibitor molecules on the metal surface can be quantified and described by the interaction energy ($E_{interaction}$), which is calculated by the following formula

$$E_{interaction} = E_{total} - (E_{surface+solution} + E_{inhibitor}) \quad (18)$$

where E_{total} is the total energy of the system, $E_{surface+solution}$ represents the sum of Fe (110) surface energy and the energy of the solution, and $E_{inhibitor}$ is the free inhibitor energy.[66] Moreover, the binding energy ($E_{binding}$) is the negative value of the interaction energy. Overall, the negative values of $E_{interaction}$ of both inhibitors indicated that adsorption spontaneously occurred and that the adsorption system was more stable.

The adsorption energies of DTZA and DPZA molecules after the protonation of the N atom on the −C═N of the heterocyclic ring are −130 and −103 kJ·mol^{-1}, respectively. Here, the negative values reflect spontaneous adsorption. The positively charged molecules have enhanced reverse chelation

https://doi.org/10.1021/acsomega.2c03545
ACS Omega 2022, 7, 32208−32224

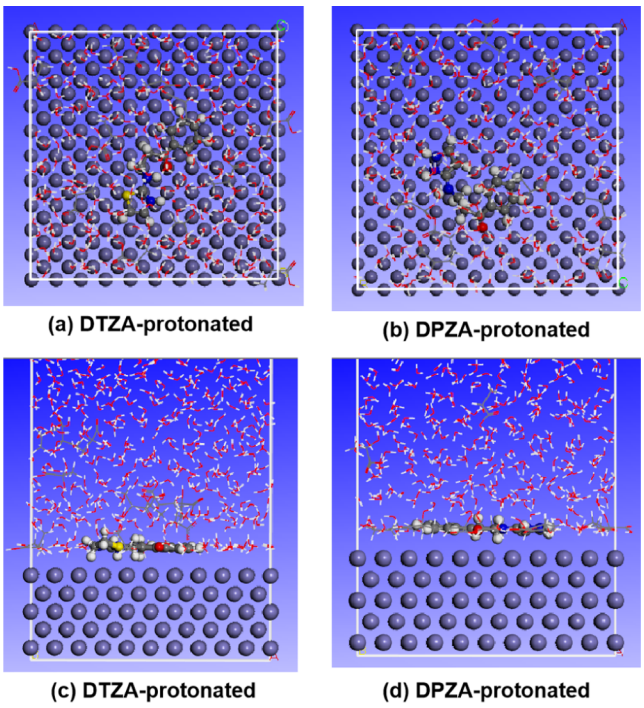

Figure 13. Equilibrium adsorption configuration of DTZA and DPZA on the Fe (110) plane: (a, b) the top view and (c, d) the side view.

ability with free electrons on the metal surface and can displace the acid anion adsorbed on the iron surface, blocking the contact of the corrosive medium to improve the corrosion inhibition performance.[67] The adsorption energy of protonated DTZA is higher than that of the neutral state. In addition, the electronegativity of the S atom of DTZA is relatively small, and it can chelate with Fe to form Fe−S with a large deposition degree. This may also contribute to its stronger adsorption capacity, yielding an excellent corrosion inhibition performance.[68]

3.11. Anticorrosion Mechanism. In the 15% lactic acid solution, both DTZA and DPZA exist in protonate forms. Based on the aforementioned experimental and theoretical analyses, it can be concluded that the anticorrosion mechanism of the inhibitors in the lactic acid solution is related to the molecular adsorption on the metal surface. As proposed in Figure 14, the positively charged five-membered heterocycles

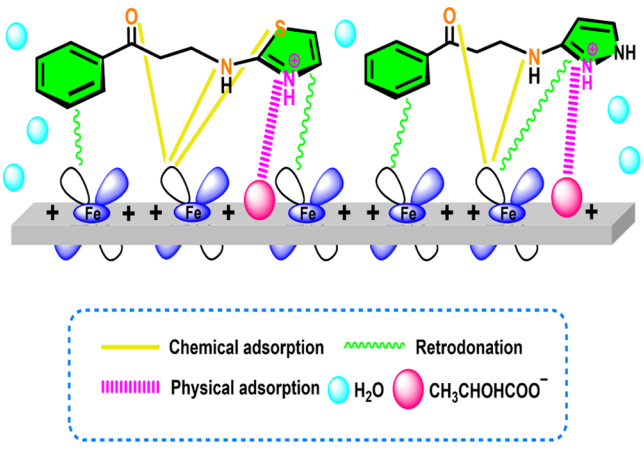

Figure 14. Inhibitor mechanisms of DTZA (a) and DPZA (b).

of the two corrosion inhibitors and the lactate ions on the iron surface produce an electrostatic attraction to form physical adsorption, which displaces the corrosive acid ions and mechanically blocks the contact between the corrosive medium and the N80 steel surface. The electron-gaining properties of the benzene ring in DTZA may also contribute to the adsorption of the inhibitor molecules through the electrostatic attraction with the negatively charged mild steel surface. Due to its stronger electrophilic characteristics, the physical adsorption of DTZA is considerably stronger than that of DPZA. Meanwhile, chemisorption is formed between inhibitors and the N80 steel surface. The carbonyl O atom, the N and S atoms, and other electron-rich centers coordinate with the empty *d* orbital on the iron surface. The presence of S in the thiazole ring enables the formation of Fe−S by the chelation of S atoms on the iron surface, strengthening the chemical adsorption of DTZA. Besides, the delocalized electrons on the benzene and heterocyclic rings of the inhibitor molecules have interactions with ionized iron, which is called retrodonation.[69] These interactions contribute together to suppress the metal dissolution in the acid solution by the formation of a protective film of the inhibitor molecules on the metal surface.

4. CONCLUSIONS

Two novel heterocyclic Mannich bases (DTZA and DPZA) were successfully prepared. A comparison of their corrosion inhibitive performance in the lactic acid solution was investigated through experimental and theoretical methods. The following conclusions can be drawn:

(1) DTZA shows satisfactory corrosion inhibitive performance, with good application potential for chelating acid-based acidizing fluids for the first time. Weight loss results indicate that the IE of DTZA on N80 steel in a 15% lactic acid solution at a dosage of 0.15 wt % reaches 97.6% at 363 K, while its analogue DPZA exhibits inferior inhibitive ability under the same environment with an IE of only 58.3%.

(2) Electrochemical results agree well with those from weight loss tests. The R_{ct} and R_p values increase with the DTZA concentration, indicating that a compact protective film was formed on the metal surface. The protective layer formed by adsorption of the DTZA molecules follows the Langmuir adsorption, which is spontaneous mixed-type adsorption.

(3) Results from SEM, AFM, XPS, and contact angle measurement images clearly support the superior protective performance of DTZA to that of DPZA. Theoretical calculations by the DFT method and MD simulations confirm that DTZA exhibits better coordination ability toward N80 steel than DPZA. The binding energies ($E_{binding}$) for DTZA and DPZA were 126.9628 and 32.2942 kJ·mol^{-1}, respectively. The existence of a sulfur atom in the DTZA molecule might be responsible for its stronger adsorption with the iron surface.

■ ASSOCIATED CONTENT

Supporting Information

The Supporting Information is available free of charge at https://pubs.acs.org/doi/10.1021/acsomega.2c03545.

^{1}H NMR and ^{13}C NMR spectra of the synthesized DPZA and DTZA; and comparison of the inhibition

https://doi.org/10.1021/acsomega.2c03545
ACS Omega 2022, 7, 32208−32224

efficiencies of DPZA and DTZA with other inhibitors (PDF)

AUTHOR INFORMATION

Corresponding Author

Xiaoyun Zhang − *Department of Materials Chemistry, College of Materials Science and Engineering, China University of Petroleum (East China), Qingdao 266580, China;* orcid.org/0000-0003-4544-3641; Email: zhangxy@upc.edu.cn

Authors

Yinhang Zhang − *Department of Materials Chemistry, College of Materials Science and Engineering, China University of Petroleum (East China), Qingdao 266580, China*

Yuxin Su − *Department of Materials Chemistry, College of Materials Science and Engineering, China University of Petroleum (East China), Qingdao 266580, China*

Xiaoyang Wang − *Sinopec Research Institute of Petroleum Engineering, Beijing 102206, China*

Renqing Lv − *Department of Chemistry, College of Chemistry and Chemical Engineering, China University of Petroleum (East China), Qingdao 266580, China*

Complete contact information is available at: https://pubs.acs.org/10.1021/acsomega.2c03545

Notes

The authors declare no competing financial interest.

ACKNOWLEDGMENTS

This work was financially supported by the National Natural Science Foundation of China (Project No. 51374230) and the Key Technologies Research and Development Program of China (Grant 2017ZX05072). Special thanks are given to Prof. Wen Fushan from the China University of Petroleum (UPC) for his help with theoretical calculations.

REFERENCES

(1) Du, J.; Xiang, K.; Zhao, L. Q.; Lan, X. T.; Liu, P. L.; Liu, Y. Corrosion inhibition of 13Cr stainless steel in HCl/HAc/HF acid solution. *Int. J. Electrochem. Sci.* **2019**, *14*, 8919−8930.

(2) Anadebe, V. C.; Nnaji, P. C.; Onukwuli, O. D.; Okafor, N. A.; Abeng, F. E.; Chukwuike, V. I.; Okoye, C. C.; Udoh, I. I.; Chidiebere, M. A.; Guo, L.; Barik, R. Multidimensional insight into the corrosion inhibition of salbutamol drug molecule on mild steel in oilfield acidizing fluid: Experimental and computer aided modeling approach. *J. Mol. Liq.* **2022**, *349*, No. 118482.

(3) Umoren, S. A.; Solomon, M. M.; Saji, V. S. Corrosion Inhibitors for Sour Oilfield Environment (H_2S Corrosion), *Corrosion Inhibitors in the Oil and Gas Industry* 2020, 229 254.

(4) de Wolf, C. A.; Nasr-El-Din, H. A.; Bouwman, A.; Bang, E. R. A.; Naylor, E. Corrosion rates of Cr- and Ni-based alloys with organic acids and chelating agents used in stimulation of deep wells. *SPE Prod. Oper.* **2017**, *32*, 208−217.

(5) Gomaa, I.; Mahmoud, M.; Kamal, M. S. Sandstone acidizing using a low-reaction acid system. *J. Energy Resour. Technol.* **2020**, *142*, No. 103008.

(6) Tariq, Z.; Hassan, A.; Al-Abdrabalnabi, R.; Aljawad, M.; Mahmoud, M. Comparative study of fracture conductivity in various carbonate rocks treated with GLDA chelating agent and HCl acid. *Energy Fuels* **2021**, *35*, 19641−19654.

(7) Wang, J.; Huang, Y. X.; Zhou, F. J.; Song, Z. Y.; Liang, X. Y. Study on reservoir damage during acidizing for high-temperature and ultra-deep tight sandstone. *J. Pet. Sci. Eng.* **2020**, *191*, No. 107231.

(8) Shi, Y.; Yu, L.; Chen, S.; He, Y.; Yang, X.; Duan, L.; Cai, J. Effects of L-glutamic acid, N, N-diacetic acid as chelating agent on acidification of carbonate reservoirs in acidic environments. *J. Nat. Gas. Sci. Eng.* **2020**, *82*, No. 103494.

(9) Al Hamad, M.; Al-Sobhi, S. A.; Onawole, A. T.; Hussein, I. A.; Khraisheh, M. Density-Functional Theory Investigation of Barite Scale Inhibition Using Phosphonate and Carboxyl-Based Inhibitors. *ACS Omega* **2020**, *5*, 33323−33328.

(10) Rabizadeh, T.; Peacock, C. L.; Benning, L. G. Investigating the Effectiveness of Phosphonate Additives in Hindering the Calcium Sulfate Dihydrate Scale Formation. *Ind. Eng. Chem. Res.* **2020**, *59*, 14970−14980.

(11) Qiang, Y.; Guo, Lei.; Li, H.; Lan, X. Fabrication of environmentally friendly Losartan potassium film for corrosion inhibition of mild steel in HCl medium. *Chem. Eng. J.* **2021**, *406*, No. 126863.

(12) Pragathiswaran, C.; Ramadevi, P.; Kumar, K. Imidazole and Al^{3+}nano material as corrosion inhibitor for mild steel in hydrochloric acid solutions. *Mater. Today: Proc.* **2021**, *37*, 2912−2916.

(13) Qiang, Y. J.; Zhi, H.; Guo, Lei.; Fu, A.; Xiang, T.; Jin, Y. Experimental and molecular modeling studies of multi-active tetrazole derivative bearing sulfur linker for protecting steel from corrosion. *J. Mol. Liq.* **2022**, *351*, No. 118638.

(14) Hrimla, M. L.; Bahsis, L.; Boutouil, A.; Laamari, M. R.; Julve, M.; Stiriba, S. Corrosion inhibition performance of a structurally well-defined 1,2,3-triazole derivative on mild steel-hydrochloric acid interface. *J. Mol. Struct.* **2021**, *1231*, No. 129895.

(15) Abd El-Lateef, H. M.; Khalaf, M. M.; Shalabi, K.; Abdelhamid, A. A. Efficient synthesis of 6,7-dihydro-5H-cyclopenta[b]pyridine-3-carbonitrile compounds and their applicability as Inhibitor films for steel alloy Corrosion: collective computational and practical approaches. *ACS Omega* **2022**, *7*, 24727−24745.

(16) Fakhry, H.; El Faydy, M.; Faydy, M. E.; Benhiba, F.; Laabaissi, T.; Bouassiria, M.; Allali, M.; Lakhrissi, B.; Oudda, H.; Guenbour, A.; Warad, I. A newly synthesized quinoline derivative as corrosion inhibitor for mild steel in molar acid medium: Characterization (SEM/EDS), experimental and theoretical approach. *Colloids Surf., A* **2021**, *610*, No. 125746.

(17) Yerlikaya, G.; Ahmad, A.; Farsak, M.; Kilig, H. K.; Kardas, G.; Kaya, S. Illuminating of mild steel/HCI interface in the presence of 5-DAT inhibitor. *J. Mol. Liq.* **2021**, *326*, No. 115380.

(18) Ayeni, A. O.; Akinyele, O. F.; Hosten, E. C.; Fakola, E. G.; Olalere, J. T.; Egharevba, G. O.; Watkins, G. M. Synthesis, crystal structure, experimental and theoretical studies of corrosion inhibition of 2-((4 -(2-hydrox y-4-m ethylbenzyl)piperazin-1-yl) methyl)-5-methylphenole. A Mannich base. *J. Mol. Struct.* **2020**, *1219*, No. 128539.

(19) El-Tabei, A. S.; Hegazy, M. A.; Bedair, A. H.; El Basiony, N. M.; Sadeq, M. A. Novel macrocyclic cationic surfactants: Synthesis, experimental and theoretical studies of their corrosion inhibition activity for carbon steel and their antimicrobial activities. *J. Mol. Liq.* **2021**, *324*, No. 116990.

(20) Selvaraj, S. D.; Krishnaveni, R.; Tamilvendan, D. Synthesis, characterization, anticorrosion and antimicrobial studies of novel 1-[anilino (phenyl) methyl] pyrimidine-2, 4, 6-trione derived from Mannich reaction and its metal complexes. *Mater. Today: Proc.* **2020**, *33*, 4271−4279.

(21) Zhang, X. Y.; Zhang, M.; Zhang, Z. S.; Li, Q.; Lv, R. Q.; Wu, W. Bis-Mannich bases as effective corrosion inhibitors for N80 steel in 15% HCl medium. *J. Mol. Liq.* **2022**, *347*, No. 117957.

(22) Mainier, F. B.; Farneze, H. N.; Serrao, L. F.; de Oliveira, B. T.; Nani, B. F. Performance of stainless steel AISI 317L in hydrochloric acid with the addition of propargyl alcohol. *Int. J. Electrochem. Sci.* **2018**, *13*, 3372−3381.

(23) Farag, A. A.; Mohamed, E. A.; Sayed, G. H.; Anwer, K. E. Experimental/computational assessments of API steel in 6 M H_2SO_4 medium containing novel pyridine derivatives as corrosion inhibitors. *J. Mol. Liq.* **2021**, *330*, No. 115705.

(24) Odewunmi, N. A.; Solomon, M. M.; Umoren, S. A.; Ali, S. A. Comparative Studies of the Corrosion Inhibition Efficacy of a Dicationic Monomer and Its Polymer against API X60 Steel Corrosion in Simulated Acidizing Fluid under Static and Hydrodynamic Conditions. *ACS Omega.* **2020**, *5*, 27057−27071.
(25) Recio, A.; Reyes, E. A.; Beuterbaugh, A. M.; Benoit, D. N. U.S. Patent US202201624982022.
(26) Umoren, S. A.; Solomon, M. M.; Obot, I. B.; Suleiman, R. K. Effect of intensifier additives on the performance of butanolic extract of date palm leaves against the corrosion of API 5L X60 carbon steel in 15 wt% HCl solution. *Sustainability* **2021**, *13*, 5569.
(27) Saady, A.; Rais, Z.; Benhiba, F.; Salim, R.; Alaoui, K. I.; Arrousse, N.; Elhajjaji, F.; Taleb, M.; Jarmoni, K.; Kandri Rodi, Y.; Warad, I.; Zarrouk, A. Chemical, electrochemical, quantum, and surface analysis evaluation on the inhibition performance of novel imidazo[4,5-b] pyridine derivatives against mild steel corrosion. *Corros. Sci.* **2021**, *189*, No. 109621.
(28) Mary, Y. S.; Mary, Y. S.; Armaković, S.; Armaković, S. J.; Krátký, M.; Vinsova, J.; Baraldi, C.; Gamberini, M. C. Concentration and solvent dependent SERS, DFT, MD simulations and molecular docking studies of a thioxothiazolidine derivative with antimicrobial properties. *J. Mol. Liq.* **2021**, *329*, No. 115582.
(29) Kumar, D.; Jain, V.; Rai, B. Imidazole Derivatives as Corrosion Inhibitors for Copper: A DFT and Reactive Force Field Study. *Corros. Sci.* **2020**, *171*, No. 108724.
(30) Solomon, M. M.; Umoren, S. A.; Quraishi, M. A.; Tripathy, D. B.; Abai, E. J. Effect of akyl chain length, flow, and temperature on the corrosion inhibition of carbon steel in a simulated acidizing environment by an imidazoline-based inhibitor. *J. Pet. Sci. Eng.* **2020**, *187*, No. 106801.
(31) Farag, A. A.; Abdallah, H. E.; Badr, E. A.; Mohamed, E. A.; Ali, A. I.; El-Etre, A. Y. The inhibition performance of morpholinium derivatives on corrosion behavior of carbon steel in the acidized formation water: Theoretical, experimental and biocidal evaluations. *J. Mol. Liq.* **2021**, *341*, No. 117348.
(32) Espinoza Vázquez, A.; López Reséndiz, L. A.; Figueroa, I. A.; Rodríguez Gómez, F. J.; Figueroa, M.; Beltrán, D. Á.; Castro, M.; Miralrio, A. Corrosion inhibition assessment on API 5L X70 steel by preussomerin G immersed in saline and saline acetic. *J. Adhes. Sci. Technol.* **2021**, *35*, 873−899.
(33) Corrales-Luna, M.; Le Manh, T.; Romero-Romo, M.; Palomar-Pardavé, M.; Arce-Estrada, E. M. 1-Ethyl 3-methylimidazolium thiocyanate ionic liquid as corrosion inhibitor of API 5L X52 steel in H_2SO_4 and HCl media. *Corros. Sci.* **2019**, *153*, 85−99.
(34) Pang, L.; Wang, Z. B.; Lu, M. H.; Lu, Y.; Liu, X.; Liu, Y. G. Inhibition performance of benzimidazole derivatives with different heteroatoms on the under-deposit corrosion of carbon steel in CO_2-saturated solution. *Corros. Sci.* **2021**, *192*, No. 109841.
(35) Zhang, G. A.; Liu, D.; Li, Y. Z.; Guo, X. P. Corrosion behavior of N80 carbon steel in formation water under dynamic supercritical CO_2 condition. *Corros. Sci.* **2017**, *120*, 107−120.
(36) Varvara, S.; Caniglia, G.; Izquierdo, J.; Bostan, R.; Găină, L.; Bobis, O.; Souto, R. M. Multiscale electrochemical analysis of the corrosion control of bronze in simulated acid rain by horse-chestnut extract as green inhibitor. *Corros. Sci.* **2020**, *165*, No. 108381.
(37) Pan, J.; Thierry, D.; Leygraf, C. Electrochemical impedance spectroscopy study of the passive oxide film on titanium for implant application. *Electrochim. Acta* **1996**, *41*, 1143−1153.
(38) Brug, G. J.; van den Eeden, A. L. G.; Sluyters-Rehbach, M.; Sluyters, J. H. The analysis of electrode impedances complicated by the presence of a constant phase element. *J. Electroanal. Chem. Interfacial Electrochem.* **1984**, *176*, 275−295.
(39) Fernandes, C. M.; Alvarez, L. X.; dos Santos, N. E.; Maldonado Barrios, A. C.; Ponzio, E. A. Green synthesis of 1-benzyl-4-phenyl-1H-1,2,3-triazole, its application as corrosion inhibitor for mild steel in acidic medium and new approach of classical electrochemical analyses. *Corros. Sci.* **2019**, *149*, 185−194.
(40) Onyeachu, I. B.; Obot, I. B.; Adesina, A. Y. Green corrosion inhibitor for oilfield application II: The time−evolution effect on the sweet corrosion of API X60 steel in synthetic brine and the inhibition performance of 2-(2-pyridyl) benzimidazole under turbulent hydrodynamics. *Corros. Sci.* **2020**, *168*, No. 108589.
(41) Mahdavian, M.; Tehrani-Bagha, A. R.; Alibakhshi, E.; Ashhari, S.; Palimi, M. J.; Farashi, S.; Javadian, S.; Ektefa, F. Corrosion of mild steel in hydrochloric acid solution in the presence of two cationic gemini surfactants with and without hydroxyl substituted spacers. *Corros. Sci.* **2018**, *137*, 62−75.
(42) Corrales Luna, M.; Le Manh, T.; Cabrera Sierra, R.; Medina Flores, J. V.; Lartundo Rojas, L.; Arce Estrada, E. M. Study of corrosion behavior of API 5L X52 steel in sulfuric acid in the presence of ionic liquid 1-ethyl 3-methylimidazolium thiocyanate as corrosion inhibitor. *J. Mol. Liq.* **2019**, *289*, No. 111106.
(43) Salman, M.; Ansari, K. R.; Srivastava, V.; Chauhan, D. S.; Haque, J.; Quraishi, M. A. Chromeno naphthyridines based heterocyclic compounds as novel acidizing corrosion inhibitors: Experimental, surface and computational study. *J. Mol. Liq.* **2021**, *322*, No. 114825.
(44) Rahimi, A.; Abdouss, M.; Farhadian, A.; Guo, L.; Neshati, J. Development of a Novel Thermally Stable Inhibitor Based on Furfuryl Alcohol for Mild Steel Corrosion in a 15% HCl Medium for Acidizing Application. *Ind. Eng. Chem. Res.* **2021**, *60*, 11030−11044.
(45) Kokalj, A. Molecular modeling of organic corrosion inhibitors: Calculations, pitfalls, and conceptualization of molecule−surface bonding. *Corros. Sci.* **2021**, *193*, No. 109650.
(46) Ituen, E.; Lin, Y. H.; Verma, C.; Alfantazi, A.; Akaranta, O.; Ebenso, E. E. Synthesis and characterization of walnut husk extract-silver nanocomposites for removal of heavy metals from petroleum wastewater and its consequences on pipework steel corrosion. *J. Mol. Liq.* **2021**, *335*, No. 116132.
(47) Yang, D.; Liu, S. H.; Shao, Y. P.; Xu, S. D.; Zhao, L. L.; Liao, Q. Q.; Ge, H. H. Electrochemical and XPS studies of alkyl imidazoline on the corrosion inhibition of carbon steel in citric acid solution *Corros. Rev.* 2016, *34*, DOI: 10.1515/corrrev-2016-0016.
(48) Prashanth, M. K.; Pradeep Kumar, C. B.; Prathibha, B. S.; Raghu, M. S.; Yogesh Kumar, K.; Jagadeesha, M. B.; Mohana, K. N.; Honnur, Krishna. Effect of OH, NH2 and OCH3 groups on the corrosion inhibition efficacy of three new 2,4,5-trisubstituted imidazole derivatives on mild steel in acidic solutions: Experimental, surface and DFT explorations. *J. Mol. Liq.* **2021**, *329*, No. 115587.
(49) Liu, Y.; Wang, Z.; Zhang, Z. Y.; Wang, Y. Y.; Cheng, J. W.; Li, H. J.; Wu, Y. C. Investigation of 3-(phenylsulfinyl)indoles self-assembled monolayer for the inhibition of iron corrosion in acidic media. *Mater. Corros.* **2022**, 1−15.
(50) Zhang, W. W.; Li, H. J.; Wang, M. R.; Wang, L. J.; Pan, Q. W.; Ji, X. B.; Qin, Y. Q.; Wu, Y. C. Tetrahydroacridines as corrosion inhibitor for X80 steel corrosion in simulated acidic oilfield water. *J. Mol. Liq.* **2019**, *293*, No. 111478.
(51) Liu, Q.; Wang, J.; Chong, Y.; Liu, J. Y. Inhibition effect of green Betaine type surfactants on Q235 steel in 1 mol·L^{-1} hydrochloric acid: The experimental and theoretical research. *J. Mol. Struct.* **2022**, *1262*, No. 133023.
(52) Li, W. P.; Luo, W.; Yu, X. K.; Ma, C. W.; Xiong, Y.; Tan, B. C.; Qiang, Y. J. Adsorption and inhibition behavior of 3-chloro-6-mercaptopyridazine towards copper corrosion in sulfuric acid. *J. Mol. Liq.* **2022**, *357*, No. 119100.
(53) Moradi Kooshksara, M.; Mohammadi, S. Investigation of the in-situ solvothermal reduction of multi-layered Graphene oxide in epoxy coating by acetonitrile on improving the hydrophobicity and corrosion resistance. *Prog. Org. Coat.* **2021**, *159*, No. 106432.
(54) Onyeachu, I. B.; Chauhan, D. S.; Ansari, K. R.; Obot, I. B.; Quraishi, M. A.; Alamri, A. H. Hexamethylene-1,6-bis(N-D-glucopyranosylamine) as a novel corrosion inhibitor for oil and gas industry: electrochemical and computational analysis. *New J. Chem.* **2019**, *43*, 7282−7293.
(55) Ammouchi, N.; Allal, H.; Belhocine, Y.; Bettazc, S.; Zouaoui, E. DFT computations and molecular dynamics investigations on conformers of some pyrazinamide derivatives as corrosion inhibitors for aluminum. *J. Mol. Liq.* **2020**, *300*, No. 112309.

https://doi.org/10.1021/acsomega.2c03545
ACS Omega 2022, 7, 32208−32224

(56) Kokalj, A.; Lozinšek, M.; Kapun, B.; Taheri, P.; Neupane, S.; Losada-Pérez, P.; Xie, C.; Stavber, S.; Crespo, D.; Renner, F. U.; Mol, A.; Milošev, A. Simplistic correlations between molecular electronic properties and inhibition efficiencies: Do they really exist? *Corros. Sci.* **2021**, *179*, No. 108856.
(57) Hashem, H. E.; Farag, A. A.; Mohamed, E. A.; Azmy, E. M. Experimental and theoretical assessment of benzopyran compounds as inhibitors to steel corrosion in aggressive acid solution. *J. Mol. Struct.* **2022**, *1249*, No. 131641.
(58) Ituen, E.; Mkpenie, V.; Lin, Y. H.; Singh, A. Inhibition of erosion corrosion of pipework steel in descaling solution using 5-hydroxytryptamine-based additives: Empirical and computational studies. *J. Mol. Struct.* **2020**, *1204*, No. 127562.
(59) Li, H.; Zhang, S. T.; Qiang, Y. J. Corrosion retardation effect of a green cauliflower extract on copper in H_2SO_4 solution: Electrochemical and theoretical explorations. *J. Mol. Liq.* **2021**, *321*, No. 114450.
(60) Yilmaz, N.; Fitoz, A.; Ergun, Ü.; Emregül, K. C. A combined electrochemical and theoretical study into the effect of 2-((thiazole-2-ylimino)methyl)phenol as a corrosion inhibitor for mild steel in a highly acidic environment. *Corros. Sci.* **2016**, *111*, 110−120.
(61) Kabanda, M. M.; Murulana, L. C.; Ozcan, M.; Karadag, F.; Dehri, I.; Obot, I. B.; Ebenso, E. E. Quantum chemical studies on the corrosion inhibition of mild steel by some triazoles and benzimidazole derivatives in acidic medium. *Int. J. Electrochem. Sci.* **2012**, *7*, 5035−5056.
(62) Pearson, R. G. Recent Advances in the Concept of Hard and Soft Acids and Bases. *J. Chem. Educ.* **1987**, *64*, 561−567.
(63) Awad, M. K.; Mustafa, M. R.; Abo Elnga, M. M. Computational simulation of the molecular structure of some triazoles as inhibitors for the corrosion of metal surface. *J. Mol. Struct.: THEOCHEM* **2010**, *959*, 66−74.
(64) Liu, Z. Y.; Lu, T.; Chen, Q. X. Intermolecular interaction characteristics of the all-carboatomic ring, cyclocarbon: Focusing on molecular adsorption and stacking. *Carbon* **2021**, *171*, 514−523.
(65) Abd El-Lateef, H. M.; Shalabi, K.; Arab, A. M.; Abdallah, Y. M. Corrosion Mitigation Performance of N80 Steel in 5% Sulfamic Acid Medium by Applying Novel Tetrahydro-1,2,4-triazines Including Triazene Moieties: Electrochemical and Theoretical Approaches. *Acs Omega* **2022**, *7*, 23380−23392.
(66) Alhaffar, M. T.; Umoren, S. A.; Obot, I. B.; Ali, S. A. Isoxazolidine derivatives as corrosion inhibitors for low carbon steel in HCl solution: experimental, theoretical and effect of KI studies. *RSC Adv.* **2018**, *8*, 1764−1777.
(67) Qiang, Y. J.; Zhang, S. T.; Guo, L.; Zheng, X. W.; Xiang, B.; Chen, S. J. Experimental and theoretical studies of four allyl imidazolium-based ionic liquids as green inhibitors for copper corrosion in sulfuric acid. *Corros. Sci.* **2017**, *119*, 68−78.
(68) Qiang, Y. J.; Li, H.; Lan, X. J. Self-assembling anchored film basing on two tetrazole derivatives for application to protect copper in sulfuric acid environment. *J. Mater. Sci. Technol.* **2020**, *52*, 63−71.
(69) Paul, P. K.; Yadav, M. Investigation on corrosion inhibition and adsorption mechanism of trazine-thiourea derivative at mild steel/HCl solution interface: Electrochemical, XPS, DFT and Monte Carlo simulation approach. *J. Electroanalytical Chem.* **2020**, *877*, No. 114599.

https://doi.org/10.1021/acsomega.2c03545
ACS Omega 2022, 7, 32208−32224